nature cell biology

A molecular mechanism to regulate lysosome motility for lysosome positioning and tubulation

Xinran Li[1], Nicholas Rydzewski[1], Ahmad Hider[1], Xiaoli Zhang[1], Junsheng Yang[2], Wuyang Wang[1], Qiong Gao[1], Xiping Cheng[1] and Haoxing Xu[1,3]

To mediate the degradation of biomacromolecules, lysosomes must traffic towards cargo-carrying vesicles for subsequent membrane fusion or fission. Mutations of the lysosomal Ca^{2+} channel TRPML1 cause lysosomal storage disease (LSD) characterized by disordered lysosomal membrane trafficking in cells. Here we show that TRPML1 activity is required to promote Ca^{2+}-dependent centripetal movement of lysosomes towards the perinuclear region (where autophagosomes accumulate) following autophagy induction. ALG-2, an EF-hand-containing protein, serves as a lysosomal Ca^{2+} sensor that associates physically with the minus-end-directed dynactin–dynein motor, while PtdIns(3,5)P_2, a lysosome-localized phosphoinositide, acts upstream of TRPML1. Furthermore, the PtdIns(3,5)P_2–TRPML1–ALG-2–dynein signalling is necessary for lysosome tubulation and reformation. In contrast, the TRPML1 pathway is not required for the perinuclear accumulation of lysosomes observed in many LSDs, which is instead likely to be caused by secondary cholesterol accumulation that constitutively activates Rab7–RILP-dependent retrograde transport. Ca^{2+} release from lysosomes thus provides an on-demand mechanism regulating lysosome motility, positioning and tubulation.

Lysosomes in animal cells accept biomaterials destined for degradation from cargo vesicles, which include endosomes, autophagosomes and phagosomes[1]. Their number, size and positioning are regulated tightly to meet constantly changing cellular needs. On completion of digestion, lysosomes can undergo lysosome exocytosis[2,3], lysosome-to-Golgi trafficking, or lysosome reformation, wherein nascent proto-lysosomes bud off from tubular lysosomal structures[4]. Vesicle trafficking (that is, fusion and fission between membranous organelles) plays a key role in these cellular processes. Membrane fusion and fission require vesicles to move in a specific direction. As is the case for other organelles, the long-range movement of lysosomes requires microtubule-based motor proteins[5,6]. Kinesin motors travel centrifugally (that is, anterogradely, or outwardly) towards the plus ends of microtubules, which are typically found at the cell periphery[5], whereas dynein motors move centripetally (that is, retrogradely, or inwardly) towards the minus ends of microtubules, which are typically perinuclear, near the microtubule-organizing centre[7,8] (MTOC). Kinesin and dynein association determines the direction of lysosome transport in response to cellular cues[5,6].

Under nutrient deprivation conditions and autophagy induction, autophagosomes form rapidly and accumulate in the perinuclear region of the cell[6]. Efficient autophagosome–lysosome fusion requires that lysosomes, which are scattered throughout the cytoplasm under resting conditions, also amass rapidly in the perinuclear region[6]. Starvation may induce cytosolic alkalization, thereby boosting minus-end-directed motility[6]. As alkalization of the cytosol as a whole would interfere with the motility of other organelles, it is likely that there are local mechanisms that regulate lysosome mobility selectively.

The motility of intracellular organelles seems to be regulated by Ca^{2+} (ref. 9). For instance, mitochondrial motility is regulated by local increases of cytosolic Ca^{2+} in an on-demand manner[9]. The primary Ca^{2+} channel in the lysosome is believed to be transient receptor potential mucolipin 1 (TRPML1, also known as MCOLN1 or ML1)[10,11]. TRPML1 participates in late-endocytic membrane trafficking, and human mutations of the gene underlie mucolipidosis type IV (ML-IV)[12], a lysosomal storage disease (LSD) characterized by lysosomal storage and autophagic defects[13,14]. Previous studies have implicated TRPML1 in phagosome–lysosome fusion[15], autophagosome–lysosome fusion, and membrane fission

[1]Department of Molecular, Cellular, and Developmental Biology, University of Michigan, 3089 Natural Science Building (Kraus), 830 North University, Ann Arbor, Michigan 48109, USA. [2]Collaborative Innovation Center of Yangtze River Delta Region Green Pharmaceuticals, College of Pharmaceutical Sciences, Zhejiang University of Technology, Hangzhou 310014, China.
[3]Correspondence should be addressed to H.X. (e-mail: haoxingx@umich.edu)

Received 26 October 2015; accepted 4 February 2016; published online 7 March 2016; DOI: 10.1038/ncb3324

© 2016 Macmillan Publishers Limited. All rights reserved

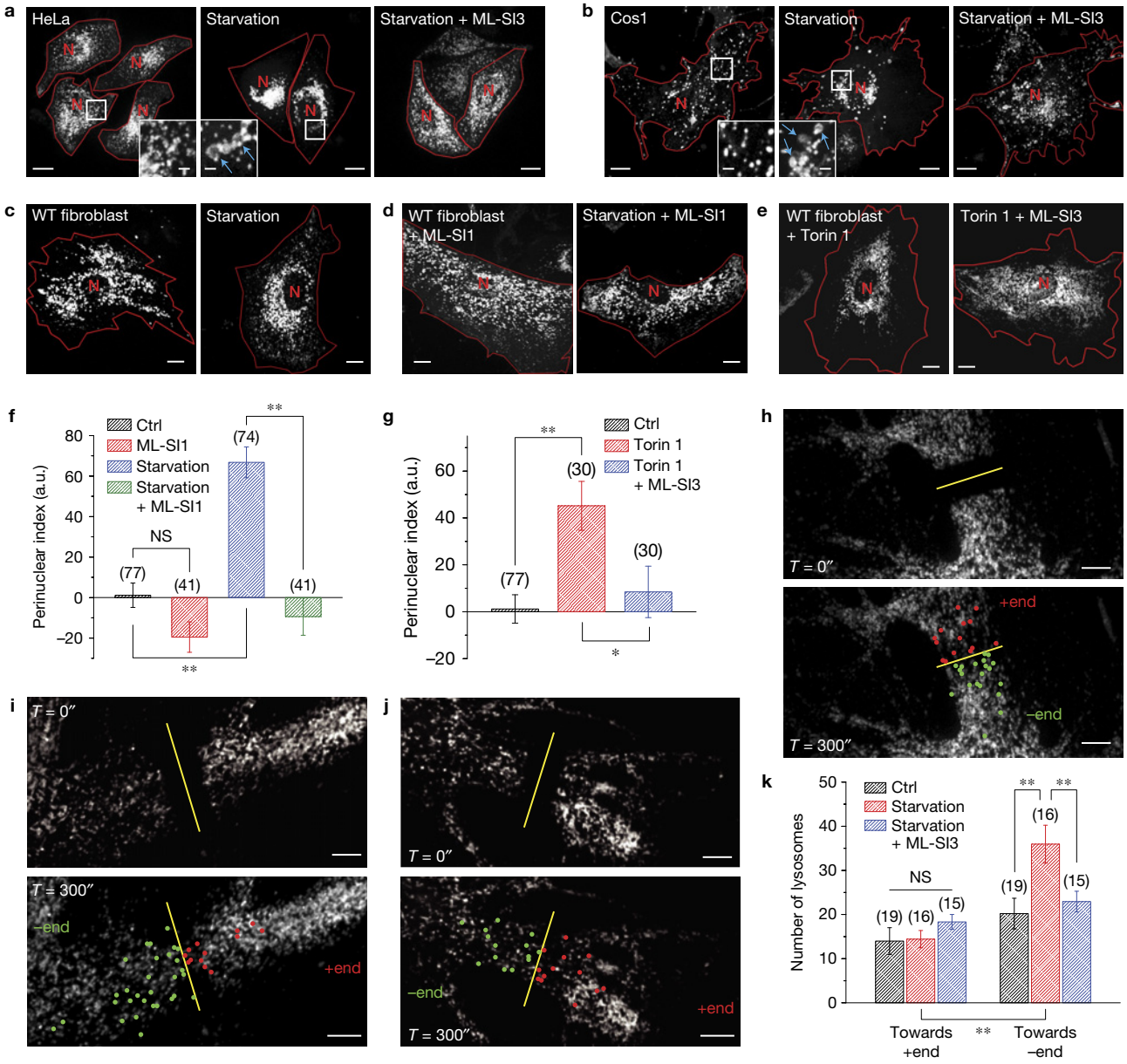

Figure 1 TRPML1 channel activity is required for acute, minus-end-directed retrograde transport of lysosomes. (**a**,**b**) Representative HeLa cells (**a**) and Cos1 cells (**b**) transfected with the late-endosome and lysosome marker Lamp1–mCherry (left) under 2 h serum starvation with (right) or without (middle) the TRPML1 inhibitor ML-SI3 (25 μM). Insets illustrate the size of lysosomes with and without starvation (same magnification, blue arrows indicate enlarged lysosomes). (**c**) Representative WT mouse fibroblasts transfected with Lamp1–mCherry (left) in 2 h starvation condition (right). (**d**) Lysosome (labelled with Lamp1) distribution in WT fibroblasts in the presence of the TRPML1 inhibitor ML-SI1 (25 μM) with (right) or without (left) starvation. (**e**) Lysosome distribution in WT fibroblasts treated with mTOR inhibitor Torin 1 (1 μM) alone or together with ML-SI3 (25 μM) for 2 h. (**f**) Quantitative analyses of lysosome distribution in the experiments shown in **c** and **d**. The intracellular distribution of Lamp1-positive vesicles was quantified as described in the Methods. Fibroblasts were chosen for most quantification analyses for their large cell area, regular shape and *ML1* KO availability. (**g**) Quantification of the groups of cells shown in **e**. (**h**–**j**) FRAP analysis of lysosome movement in WT fibroblasts without any treatment (**h**), with 15–30 min starvation (**i**), or with starvation in the presence of 25 μM ML-SI3 (**j**). Snap images immediately after (top panels) or 5 min after (bottom panels) photobleaching are shown. Lysosomes that travelled across the midline of the photobleached region (yellow line) towards the nucleus (retrograde) are labelled green; those moving away from the nucleus (anterograde) are labelled red. (**k**) Quantification of the lysosomes in **h**–**j** undergoing retrograde or anterograde transport. Red lines in images outline cell boundaries and the red 'N' marks the nucleus. Graphed data are presented as means ± s.e.m.; the numbers of cells (*n*) used for quantification were pooled across at least three independent experiments, and are shown in the parentheses (for each sample group, no sample was excluded). $^{*}P < 0.05$, $^{**}P < 0.01$ in ANOVA. NS, not significant. Scale bars, 10 μm, and 2 μm for insets.

from endolysosomes[16]. However, some of the observed trafficking defects in ML-IV cells may be caused by secondary mechanisms due to chronic lysosome storage[16]. In the current study, the role of lysosomal Ca^{2+} and TRPML1 in regulating lysosome motility was examined by manipulating TRPML1 activity acutely through specific synthetic agonists or antagonists.

© 2016 Macmillan Publishers Limited. All rights reserved

RESULTS

TRPML1 is necessary for on-demand (acute) retrograde transport of lysosomes towards the MTOC

We investigated lysosome positioning in a morphologically diverse series of mammalian cells, including HeLa cells, Cos1 cells and primary mouse fibroblasts. In cells transfected with Lamp1–mCherry, a marker of late endosomes and lysosomes (referred to as 'lysosomes' for simplicity hereafter), lysosomes were scattered throughout the cytoplasm under normal culture conditions (Fig. 1a–c and Supplementary Fig. 1a,b). Serum starvation triggered rapid autophagy and generation of autophagosomes, evidenced by the formation of LC3 puncta (Supplementary Fig. 1e). Autophagosomes accumulated primarily in the perinuclear region[17,18] (Supplementary Fig. 1e). Consistent with previous studies[6], on starvation, lysosomes were redistributed rapidly towards the perinuclear region, especially the MTOC (Fig. 1a–c,f; Supplementary Fig. 1b–d). It has been suggested that this redistribution may promote membrane fusion between lysosomes and autophagosomes[17]. Indeed, Lamp1-positive compartments in the perinuclear region of starved cells were often larger than those in fed cells (Fig. 1a,b, insets), suggesting that they were secondary lysosomes, most likely autolysosomes[4]. When autophagy was triggered by Torin 1 through inhibition of mTOR (ref. 19), lysosomes also underwent perinuclear redistribution (Fig. 1e,g).

We next analysed the directional movement of lysosomes using fluorescence recovery after photobleaching (FRAP). Under resting conditions, roughly equal numbers of lysosomes travelled retrogradely and anterogradely in mouse fibroblasts (Fig. 1h,k and Supplementary Video 1). Brief (30 min) starvation resulted in a selective increase in retrograde transport of lysosomes without affecting anterograde transport (Fig. 1i,k and Supplementary Video 2). Hence, starvation may upregulate retrograde migration mechanisms, producing a redistribution of lysosomes to the perinuclear area.

Lysosome motility, in both retrograde and anterograde directions, was reduced significantly in mouse fibroblasts that were treated with a membrane-permeable form of the fast Ca^{2+} chelator BAPTA-AM (ref. 16; Supplementary Video 3), suggesting that Ca^{2+} plays an essential role in the regulation of lysosome motility. Given the delayed delivery of autophagic substrates to lysosomes and autophagosome accumulation in TRPML1-deficient cells[20,21], we investigated the role of TRPML1 in Ca^{2+}-dependent lysosome mobility by manipulating TRPML1 activity acutely with synthetic TRPML1 inhibitors (ML-SIs; see Supplementary Fig. 2a)[3,22].

The perinuclear accumulation of lysosomes under short-term starvation was blocked by ML-SI1 or ML-SI3, two structurally unrelated ML-SIs (refs 3,23; Fig. 1a–d,f), suggesting that the effects were specific to TRPML1. TRPML1 inhibition under short-term starvation also led to the accumulation of autophagosomes (Supplementary Fig. 1f,g), suggesting a role for TRPML1 activity in the delivery of lysosomes during autolysosome formation. Consistent with this prediction, FRAP analysis revealed that starvation-induced retrograde migration of lysosomes was reduced by ML-SI3 (Fig. 1j,k and Supplementary Video 4). Likewise, when autophagy was triggered by mTOR inhibitors[19], the perinuclear redistribution of lysosomes was suppressed on acute inhibition of TRPML1 (Fig. 1e,g).

Starvation has been shown to cause rapid cytosolic alkalization in HeLa cells, which is sufficient to induce perinuclear localization of lysosomes[6]. Also, whole-endolysosome TRPML1 currents were facilitated by an alkaline cytosolic pH (Supplementary Fig. 2b). Interestingly, inhibition of TRPML1 also suppressed retrograde migration of lysosomes induced by acute cytosolic alkalization (Supplementary Fig. 2c–f). Hence, TRPML1 is required to drive on-demand retrograde migration of lysosomes in response to autophagy induction and cytosolic alkalization.

TRPML1 activation is sufficient to promote Ca^{2+}-dependent retrograde transport of lysosomes

Next, we tested whether artificial activation of TRPML1 is sufficient to induce retrograde migration and perinuclear accumulation of lysosomes. When mouse fibroblasts, Cos1 cells or HeLa cells were treated with synthetic TRPML1 agonists[23,24] (ML-SAs), perinuclear localization of lysosomes was markedly increased (Fig. 2a–c,g and Supplementary Fig. 3a). Overexpression of TRPML1, but not the related TRPML2 or TRPML3, also resulted in perinuclear localization (Fig. 2d,g and Supplementary Fig. 3b–e). The effect of overexpression could be readily reversed by BAPTA-AM (Fig. 2e,h) or TRPML1 inhibitors[22] (Fig. 2f,i and Supplementary Fig. 3f,g).

In FRAP analyses, as well as in time-lapse imaging, acute application of ML-SA1 ($\leq$30 min) increased minus-end-directed migration of lysosomes significantly (Fig. 2j,k and Supplementary Videos 5–7). In contrast, the distribution of mitochondria was not affected by ML-SA1 application (Supplementary Fig. 3h–j). Conversely, time-lapse imaging showed that in TRPML1-overexpressing cells, ML-SI3 application resulted in the dispersal of lysosomes (Supplementary Video 8). Collectively, these results suggest that increasing TRPML1 activity is sufficient to induce perinuclear redistribution and retrograde transport of lysosomes.

Chronic effects of cholesterol accumulation on lysosome distribution

Lysosomes are distributed perinuclearly in many LSD cells[2,16], including TRPML1 knockout (*ML1* KO) fibroblasts (Fig. 3a–f). This distribution is opposite to that seen with transient TRPML1 inhibition. When we increased the treatment time of the TRPML1 inhibitors to >6 h and up to 48 h, lysosomes became progressively more perinuclear in wild-type (WT) fibroblasts, resembling the distribution in *ML1* KO fibroblasts (Supplementary Fig. 4a–c). Given the established role of cholesterol in promoting minus-end motility of lysosomes in cooperation with Rab7 and RILP (refs 25,26), and given that cholesterol accumulates in lysosomes in a variety of LSDs (ref. 27) including ML-IV (ref. 14; Supplementary Fig. 4e), we investigated whether cholesterol accumulation, caused by chronic lysosomal dysfunction, could account for the abnormal lysosome mobility and distribution in ML-IV and other LSDs.

Significant elevation of cholesterol was observed in the lysosomes of *ML1* KO fibroblasts, as well as in WT fibroblasts that were treated with ML-SI3 for a prolonged period of time (>6 h), but not in WT cells treated with ML-SI3 for a short (1 h) duration (Fig. 3g,h,j). Hence, cholesterol accumulation in *ML1* KO cells might have promoted minus-end motility of lysosomes independent of TRPML1 (ref. 26). Indeed, reduction of cholesterol with simvastatin[26] (Fig. 3g–i,k) resulted in more peripherally local-

© 2016 Macmillan Publishers Limited. All rights reserved

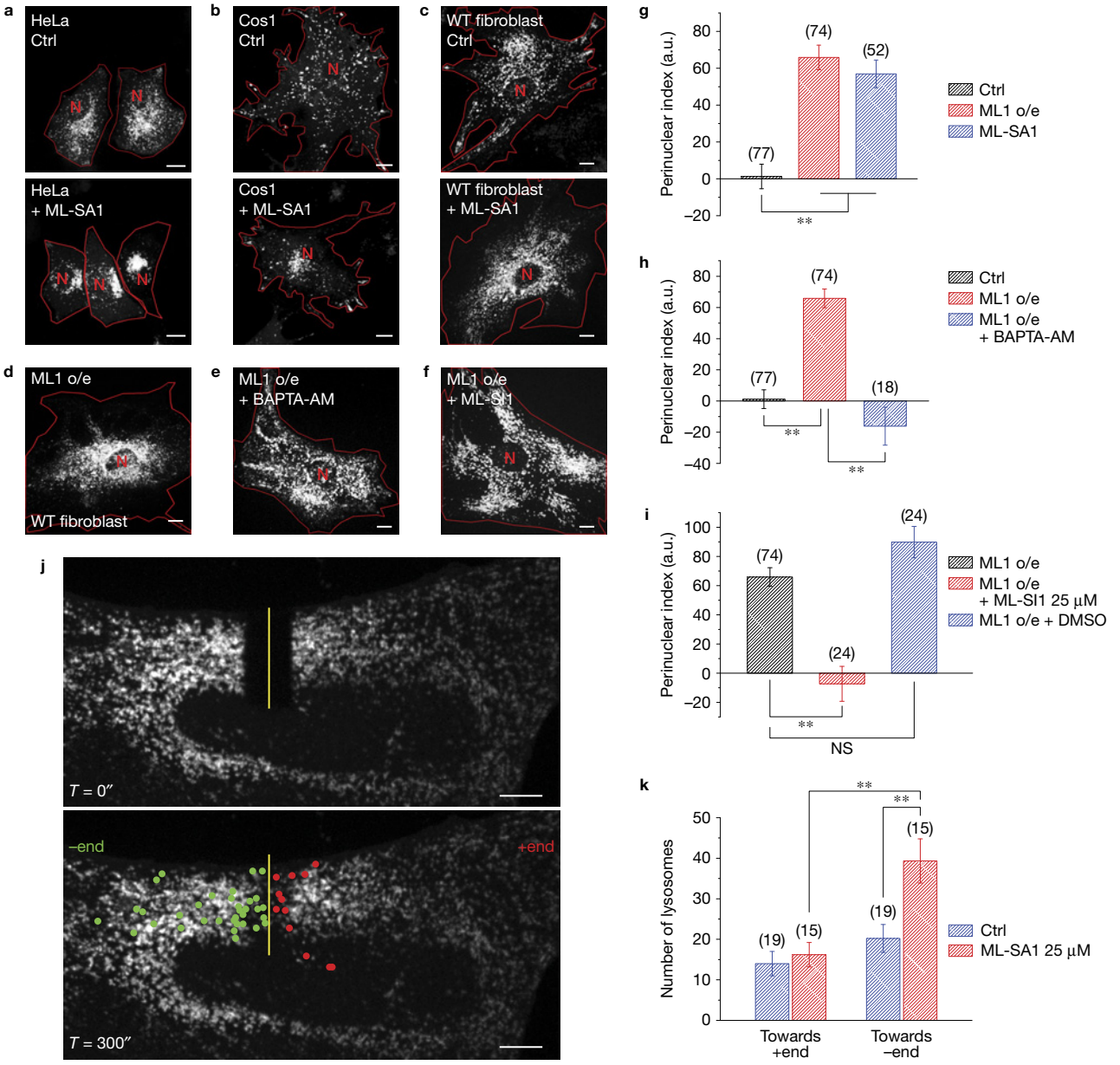

Figure 2 Activation of TRPML1 is sufficient to promote Ca^{2+}-dependent retrograde migration of lysosomes. (**a**–**c**) HeLa cells (**a**), Cos1 cells (**b**) and WT fibroblasts (**c**) with (bottom) and without (top) 25 μM ML-SA1 for 2 h. (**d**–**f**) Lysosome distribution in TRPML1-overexpressing (o/e) WT fibroblasts (**d**) treated with 10 μM BAPTA-AM for 1 h (**e**) or 25 μM ML-SI1 for 2 h (**f**). (**g**) Quantification of the lysosome distribution in the experiments shown in **c** and **d**. (**h**) Quantification of the experimental group shown in **e**. (**i**) Quantification of the experimental group shown in **f**. DMSO, dimethylsulphoxide. (**j**) FRAP analysis of lysosome retrograde transport on ML-SA1 application. (**k**) Quantification of the lysosomes shown in **j** undergoing retrograde and anterograde transport after photobleaching. Red lines delineate cell boundaries and the red 'N' marks the nucleus. Graphed data are presented as means ± s.e.m.; the numbers of cells (*n*) used for quantification were pooled across at least three independent experiments and are shown in the parentheses (for each sample group, no sample was excluded). $^{**}P < 0.01$ in ANOVA. NS, not significant. Scale bars, 10 μm.

ized lysosomes in *ML1* KO fibroblasts (Fig. 3a,b), as well as in fibroblasts from *NPC1* KO mice (Fig. 3c,e), a mouse model of the cholesterol storage disease Niemann–Pick type C (NPC)[27,28]. Taken together, perinuclear lysosome localization observed with long-term loss of TRPML1 activity or in other LSDs may be due to secondary accumulation of cholesterol. Therefore, acute manipulations are needed to investigate the mechanisms of lysosome mobility.

TRPML1 promotes retrograde trafficking independent of the Rab7–RILP pathway

Cholesterol has been previously shown to promote retrograde transport of lysosomes by facilitating the Rab7–RILP pathway through the cholesterol sensor protein ORP1L (refs 26,29). In WT fibroblasts, overexpression of the constitutively active form of Rab7 (Rab7-Q67L)[30], as well as the Rab7 effector, RILP (ref. 31), resulted in perinuclear accumulation of lysosomes (Fig. 4a–d).

© 2016 Macmillan Publishers Limited. All rights reserved

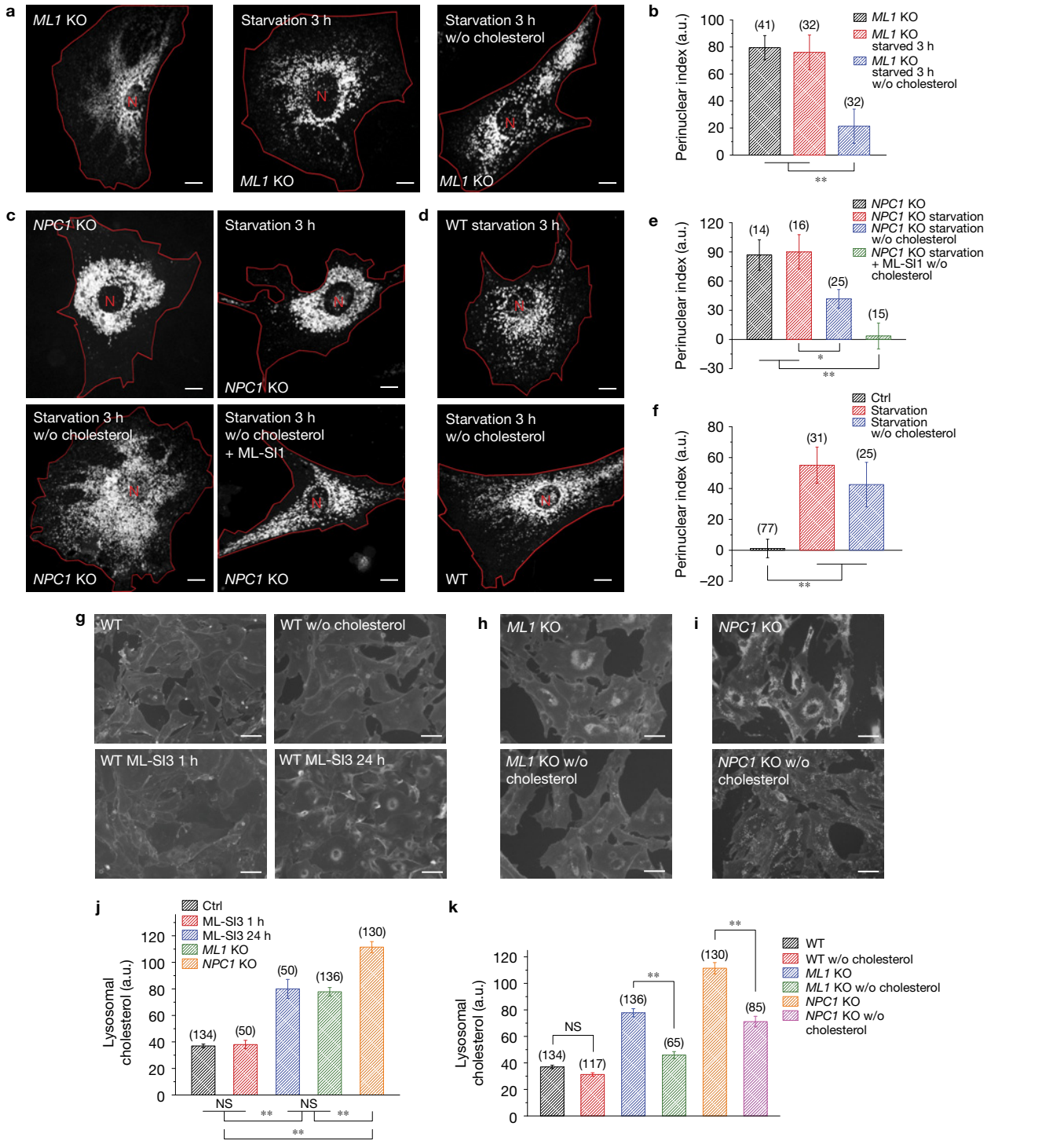

Figure 3 Cholesterol accumulation causes perinuclear localization of lysosomes in LSDs. (**a**) Representative images showing Lamp1–mCherry-transfected *ML1* KO fibroblasts in starved cells that were treated with simvastatin and mevalonolactone to deplete cholesterol. (**b**) Quantification of the groups shown in **a**. (**c**) Representative images showing Lamp1–mCherry-transfected *NPC1* KO fibroblasts (upper left), starved for 3 h (upper right), starved with cholesterol depletion (bottom left), or starved with cholesterol depletion in the presence of 25 μM ML-SI1 (bottom right). (**d**) Effect of cholesterol depletion on starvation-induced lysosome redistribution in WT fibroblasts. (**e**) Quantification of the groups shown in **c**. (**f**) Quantification of the observations shown in **d**. (**g**) Filipin staining of WT fibroblasts (upper left) and WT fibroblasts depleted of cholesterol with simvastatin (upper right), WT fibroblasts treated with 25 μM ML-SI3 for 1 h (bottom left) or 24 h (bottom right). (**h**) *ML1* KO fibroblasts with (bottom) or without (upper) cholesterol depletion. (**i**) *NPC1* KO fibroblasts with (bottom) or without (upper) cholesterol depletion. (**j**) Quantitative comparison of filipin staining in WT fibroblasts treated for different durations with ML-SI3 versus *ML1* KO and *NPC1* KO fibroblasts. (**k**) Quantification of the filipin staining in WT, *ML1* KO and *NPC1* KO fibroblasts with or without cholesterol depletion. Red lines in images outline cell boundaries and the red 'N' marks the nucleus. Graphed data are presented as means ± s.e.m.; the numbers of cells (*n*) used for quantification were pooled across at least three independent experiments and are shown in the parentheses. $^{*}P<0.05$, $^{**}P<0.01$ in ANOVA. NS, not significant. Scale bars, 10 μm for **a**,**c**,**d** and 50 μm for **g**–**i**.

© 2016 Macmillan Publishers Limited. All rights reserved

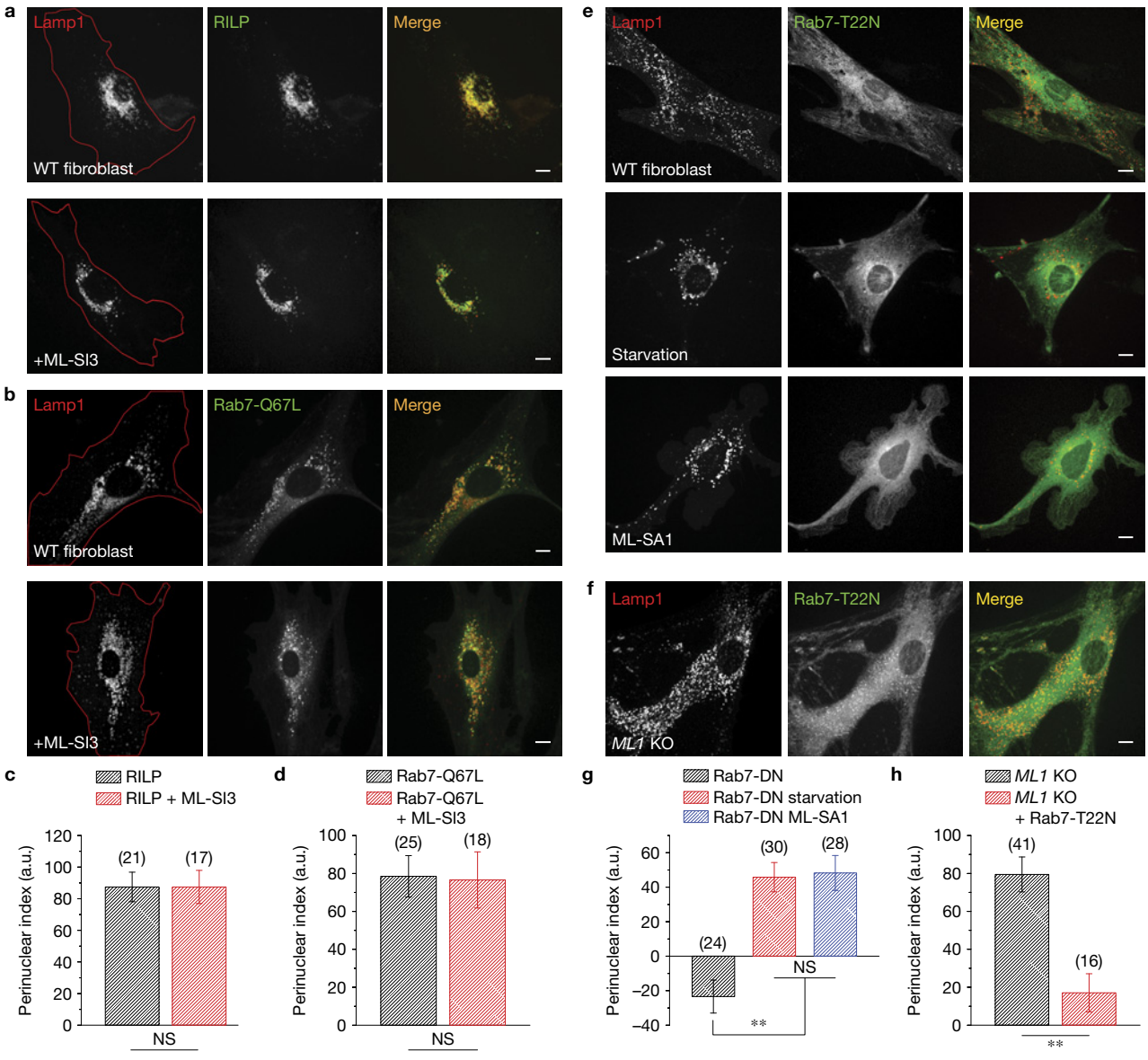

Figure 4 TRPML1 promotes retrograde migration of lysosomes independent of the Rab7–RILP pathway. (**a**,**b**) Representative images showing WT fibroblasts overexpressing Lamp1–mCherry and RILP–GFP (**a**) or Rab7-Q67L–GFP (**b**) in the presence or absence of 25 μM ML-SI3 for 2 h. (**c**) Quantification of the groups shown in **a**. (**d**) Quantification of the groups shown in **b**. (**e**) Representative images showing WT fibroblasts transfected with Lamp1–mCherry and Rab7-T22N–GFP, and then left untreated (upper panels), serum starved for 2 h (middle panels), or incubated with 25 μM ML-SA1 for 2 h (bottom panels). (**f**) Representative images showing *ML1* KO fibroblasts overexpressing Lamp1–mCherry and Rab7-T22N–GFP. (**g**) Quantification of the groups shown in **e**. (**h**) Quantification of the group shown in **f**. Red lines in images outline cell boundaries. Graphed data are presented as means ± s.e.m.; the numbers of cells (*n*) used for quantification were pooled across at least three independent experiments and are shown in the parentheses. $^{**}P < 0.01$ in ANOVA. NS, not significant. Scale bars, 10 μm.

However, ML-SI3 failed to reverse the perinuclear localization under these conditions (Fig. 4a–d). Overexpression of dominant-negative Rab7 (Rab7-T22N)[31,32] did not prevent perinuclear accumulation of lysosomes under acute starvation, or under ML-SA1 application (Fig. 4e,g), but readily suppressed the perinuclear accumulation under prolonged inhibition of TRPML1 or in *ML1* KO fibroblasts (Fig. 4f,h and Supplementary Fig. 4d). Hence, the perinuclear localization of lysosomes observed in *ML1* KO cells is likely to be due to the activation of the Rab7–RILP–ORP1L pathway by cholesterol. Taken together, these results suggest that TRPML1 and cholesterol–Rab7–RILP most likely function in two separate pathways to promote retrograde transport of lysosomes.

The role of PtdIns(3,5)P_2 in retrograde trafficking of lysosomes

Phosphatidylinositol-3,5-bisphosphate (PtdIns(3,5)P_2) is a lysosome-localized phosphoinositide[33] that regulates autophagy during nutrient deprivation[34] and is the only known endogenous agonist of TRPML1 (ref. 2). It binds directly to several positively charged residues in the amino terminus of TRPML1, thereby activating the channel[35,36]. Prolonged PtdIns(3,5)P_2 depletion leads to severe

© 2016 Macmillan Publishers Limited. All rights reserved

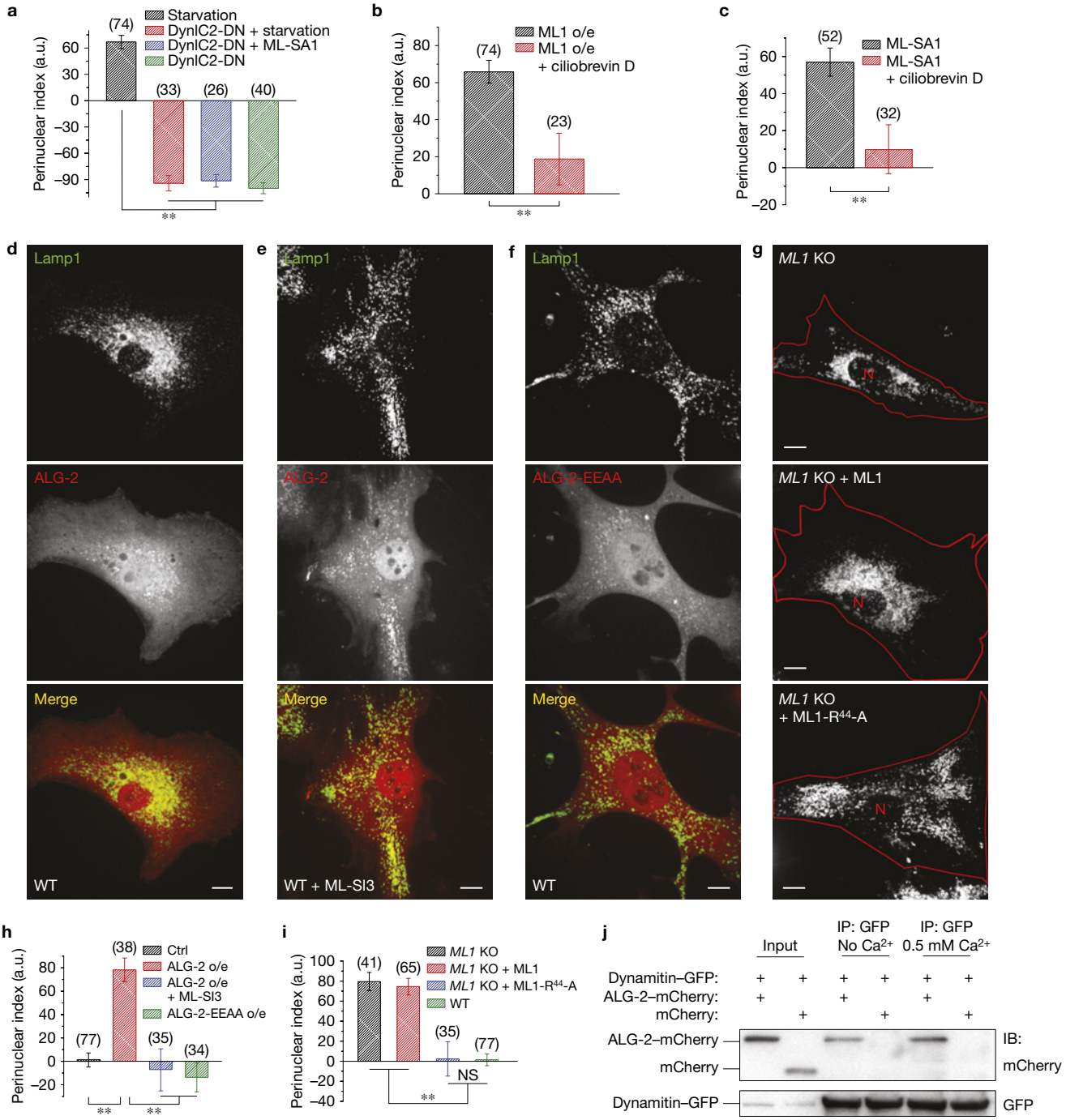

Figure 5 ALG-2 interacts with dynein complexes to mediate TRPML1-dependent minus-end-directed transport of lysosomes. (**a**) Quantification of the effect of dominant-negative dynein intermediate chain 2 (DynIC2-DN) on the distribution of lysosomes under different conditions (see Supplementary Fig. 5j–l). (**b**) Quantification of the effect of 20 μM ciliobrevin D (1 h) on lysosome distribution with or without TRPML1 overexpression (see Supplementary Fig. 5m). (**c**) Quantification of the effect of ciliobrevin D (1 h) on lysosome distribution in the presence or absence of 25 μM ML-SA1 (see Supplementary Fig. 5n). (**d**) Lysosome distribution in WT fibroblasts co-transfected with Lamp1–GFP and mCherry–ALG-2. (**e**) Lysosome distribution in mCherry–ALG-2-transfected cells treated with ML-SI3 (25 μM) for 1 h. (**f**) Lysosome distribution in WT fibroblasts co-transfected with Lamp1–GFP and mCherry–ALG-2-EEAA ($E^{47}A$-$E^{114}A$). (**g**) Lysosome distribution in *ML1* KO fibroblasts transfected with Lamp1–mCherry alone (top), Lamp1–mCherry + GFP–TRPML1 (middle), or Lamp1–mCherry + GFP–TRPML1-R^{44}-A (bottom). (**h**) Quantification of the lysosome distribution in the experiments shown in **d**–**f**. (**i**) Quantification of the groups shown in **g**. (**j**) Co-immunoprecipitation of ALG-2 and dynamitin in Cos-1 cells doubly transfected with mCherry–ALG-2 and GFP–dynamitin, in the absence or presence of 0.5 mM Ca^{2+} in the lysis buffer. Cell lysates were directly loaded (input), or immunoprecipitated with either anti-GFP or anti-mCherry antibody, and then blotted against GFP. Red lines in images outline cell boundaries and the red 'N' marks the nucleus. Graphed data are presented as means ± s.e.m.; the numbers of cells (*n*) used for quantification were pooled across at least three independent experiments and are shown in the parentheses. $^{**}P < 0.01$ in ANOVA. NS, not significant. Scale bars, 10 μm. Unprocessed original scans of blots are shown in Supplementary Fig. 9.

© 2016 Macmillan Publishers Limited. All rights reserved

enlargement of lysosomes that occupy most of the cytosolic space[37,38]. Short-term (1 h) treatment with YM 201636 or apilimod (1 μM; well-established synthetic inhibitors of the PtdIns(3,5)P_2 and PtdIns(5)P-synthesizing enzyme PIKfyve; refs 37–40) resulted in a small but significant increase in the peripheral distribution of lysosomes in non-starved cells (Supplementary Fig. 5a,e), and effectively suppressed the retrograde migration of lysosomes in acutely nutrient-deprived cells (Supplementary Fig. 5b,f) or Torin-1-treated cells (Supplementary Fig. 5c,g). mTOR inhibition by Torin 1 did not directly activate TRPML1 (see preliminary results in Supplementary Fig. 5p,q).

Short-term application of ML-SA1 increased perinuclear localization of lysosomes in YM-201636-treated cells (Supplementary Fig. 5a,e), suggesting that PtdIns(3,5)P_2 regulates lysosome distribution through TRPML1. Consistently, overexpression of a PtdIns(3,5)P_2-insensitive mutant form, TRPML1-7Q (ref. 35), did not result in the perinuclear lysosome accumulation that occurred with WT TRPML1 overexpression (Supplementary Fig. 5d,h). ML-SA1 treatment, however, increased perinuclear localization of lysosomes reliably in TRPML1-7Q-expressing cells (Supplementary Fig. 5d,h). Taken together, these results suggest that the PtdIns(3,5)P_2 sensitivity of TRPML1 is essential for retrograde lysosome transport under normal physiological conditions, and that synthetic agonists can be used as substitutes for PtdIns(3,5)P_2 in this function.

TRPML1-dependent retrograde migration of lysosomes through cytoplasmic dynein motors

In mammalian cells, long-range transport of organelles is mediated by microtubule-based motor proteins[5,29,41], including plus-end-directed kinesins and minus-end-directed dynein complexes. KIF5B and cytoplasmic dynein I (DynC1H1) transport lysosomes in mammalian cells[42–45]. Overexpression of dominant-negative KIF5B (KIF5B-DN)[46] in mouse fibroblasts produced juxtanuclear clustering of lysosomes, whereas overexpression of dominant-negative cytoplasmic dynein intermediate chain 2 (DynIC2-DN)[47] resulted in a predominantly peripheral localization of lysosomes (Fig. 5a and Supplementary Fig. 5i,j,o). Expression of DynIC2-DN inhibited starvation-induced or ML-SA1-induced perinuclear lysosomal localization completely (Fig. 5a and Supplementary Fig. 5k,l). DynIC2-DN overexpression also shifted cholesterol-accumulating puncta structures to the cell periphery in *ML1* KO fibroblasts without correcting the cholesterol accumulation phenotype per se (Supplementary Fig. 4f). Two-hour exposure to the dynein inhibitor ciliobrevin D (refs 48,49) also reversed the perinuclear distribution caused by ML-SA1 or TRPML1 overexpression (Fig. 5c and Supplementary Fig. 5m,n). Collectively, TRPML1-dependent retrograde trafficking of lysosomes may require cytoplasmic dynein activity.

ALG-2 acts as a downstream effector of TRPML1 in promoting minus-end lysosomal motility

We next investigated whether apoptosis-linked gene 2 (ALG-2, also known as PDCD6), a cytosolic protein with five EF-hand motifs[50] that interact directly with TRPML1 in a Ca^{2+}-dependent manner[51], might mediate the Ca^{2+} dependence of lysosome motility. Indeed, ALG-2 overexpression in fibroblasts resulted in a pronounced perinuclear distribution of lysosomes (Fig. 5d,h and Supplementary Fig. 6d). In contrast, overexpression of synaptotagmin-VII, another lysosomal Ca^{2+} sensor[2], did not affect lysosome distribution (Supplementary Fig. 6a–c). Likewise, a Ca^{2+}-binding-defective EF-hand mutant[51] (ALG-2-E^{47}A-E^{114}A, or ALG-2-EEAA) also had no effect (Fig. 5f,h). Moreover, the ALG-2 effect was abolished by TRPML1 inhibition (Fig. 5e,h). On the other hand, activation of TRPML1 with ML-SA1 increased the co-localization of GFP–ALG-2 with Lamp1–mCherry (Supplementary Fig. 6d–f). Therefore, ALG-2 may serve as a Ca^{2+} effector of TRPML1 to promote perinuclear distribution of lysosomes.

ALG-2 interacts with TRPML1 through a stretch of three amino acids (Arg44, Leu45 and Lys46) in the N terminus of TRPML1. Mutations of these residues (for example, TRPML1-R^{44}-A or TRPML1-R^{44}LK-AAA) attenuate or abolish TRPML1–ALG-2 interaction[51]. As TRPML1-R^{44}-A generated whole-endolysosome currents comparable to the WT channel (Supplementary Fig. 7a–c), we used TRPML1-R^{44}-A for lysosome mobility studies. As mentioned above, lysosomes in *ML1* KO fibroblasts exhibited a perinuclear pattern, presumably because of cholesterol-dependent retrograde trafficking (Fig. 3). Overexpression of WT TRPML1 in *ML1* KO fibroblasts did not suppress the perinuclear distribution of lysosomes (Fig. 5g,i), but rather resulted in a lysosome pattern similar to that produced by overexpression of TRPML1 in WT cells because of the constitutive activity of overexpressed TRPML1 (Supplementary Fig. 7d,f,g). In contrast, overexpression of TRPML1-R^{44}-A readily reversed the perinuclear distribution of lysosomes completely in *ML1* KO cells (Fig. 5d,f), and rescued cholesterol accumulation (Supplementary Fig. 7e). Importantly, ALG-2 pulled down dynamitin, a dynactin complex component[29], in co-immunoprecipitation assays in a Ca^{2+}-independent manner (Fig. 5j and Supplementary Fig. 7h–j). Hence, ALG-2 may link TRPML1 activation and lysosomal Ca^{2+} release with dynein motors in retrograde trafficking of lysosomes.

We next generated *ALG-2* KO HeLa cells using the CRISPR/Cas9 system[52] (Fig. 6a,b). At resting conditions, *ALG-2* KO HeLa cells exhibited a dispersed lysosome pattern, similar to WT cells (Fig. 6c,h). In sharp contrast to WT cells, on ML-SA1 application or acute starvation, the distribution of lysosomes in *ALG-2* KO cells remained peripheral (Fig. 6d,e,h). These data strongly suggest that ALG-2 is required for the TRPM1-dependent retrograde migration of lysosomes. Conversely, perinuclear accumulation of lysosomes caused by RILP overexpression was not blocked by *ALG-2* KO (Fig. 6f,g). Interestingly, in *ALG-2* KO cells, whereas the basal LC3-II levels were elevated compared with WT cells, starvation-induced degradation of LC3-II was blocked (Fig. 6i,j). Collectively, these results suggest that the TRPML1–ALG-2-dependent retrograde transport is required for efficient autophagic clearance.

TRPML1 and lysosomal Ca^{2+} are required for lysosome tubulation

Lysosome tubules serve as a platform for lysosome reformation, a process through which membrane lipids and proteins are recycled via membrane fission[4]. Lysosome reformation is especially prominent when lysosomes are undergoing rapid consumption, such as during phagocytosis or prolonged starvation[4,53]. We found that loss of activity of kinesin or dynein, both of which are implicated in lysosome reformation[53], abolished lysosome tubulation during autophagic lysosome reformation (Supplementary Fig. 8a).

© 2016 Macmillan Publishers Limited. All rights reserved

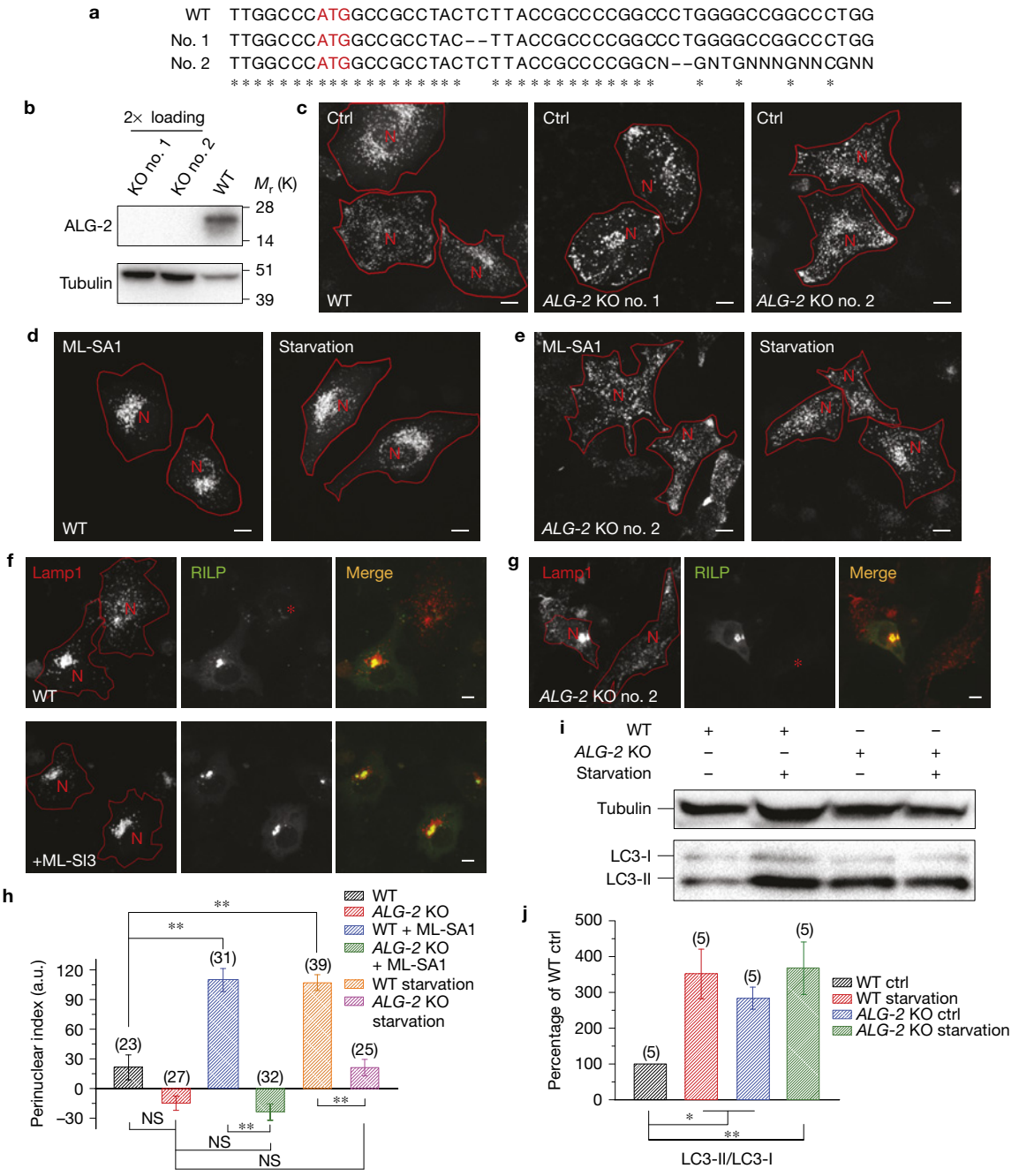

Figure 6 ALG-2 is required for the TRPML1-promoted acute retrograde migration of lysosomes. (**a**) DNA sequencing results of the two *ALG-2* CRISPR KO HeLa cell lines; the red 'ATG' indicates the start codon. Mutant no. 1 had a 2 bp deletion on all chromosomes, and mutant no. 2 had various lengths of out-of-frame deletions. (**b**) Western blot confirmation of the *ALG-2* KO. (**c**) Representative images showing Lamp1–mCherry distribution of WT (left) and the two mutant lines in complete medium without any treatment. (**d**,**e**) WT (**d**) and *ALG-2* KO (**e**) cells under 2 h of 25 μM ML-SA1 treatment (left), or under 2 h of serum starvation (right). Mutant no. 2 was chosen for further studies on the basis of its more extended morphology. (**f**,**g**) WT (**f**) and *ALG-2* KO (**g**) cells overexpressing Lamp–mCherry and RILP–GFP in the presence of 25 μM ML-SI3 for 2 h. Red asterisks in RILP panels indicate cells not expressing RILP–GFP. (**h**) Quantification of the groups shown in **c**–**e**. (**i**,**j**) Western blot analysis of endogenous LC3 in WT or *ALG-2* KO HeLa cells on 2 h starvation. LC3-II over LC3-I ratios normalized to WT control cells from five independent experiments were quantified in **j**. Red lines in images outline cell boundaries and the red 'N' marks the nucleus. Graphed data are presented as means ± s.e.m.; the numbers of cells (*n*) used for quantification were pooled across at least three independent experiments and are shown in the parentheses. $^{*}P<0.05$, $^{**}P<0.01$ in ANOVA. NS, not significant. Scale bars, 10 μm. Unprocessed original scans of blots are shown in Supplementary Fig. 9.

Lysosome tubulation occurs under various conditions in different cell types, for examples, during prolonged starvation[4] in fibroblasts and NRK cells (Fig. 7a,b and Supplementary Fig. 8b,c), during LPS activation in macrophages[53] (Fig. 7c,d), and constitutively in CV1 cells (Fig. 7e,f). Interestingly, *ML1* KO or acute inhibition of TRPML1 abolished lysosome tubulation in all conditions (Fig. 7b,d,f and

© 2016 Macmillan Publishers Limited. All rights reserved

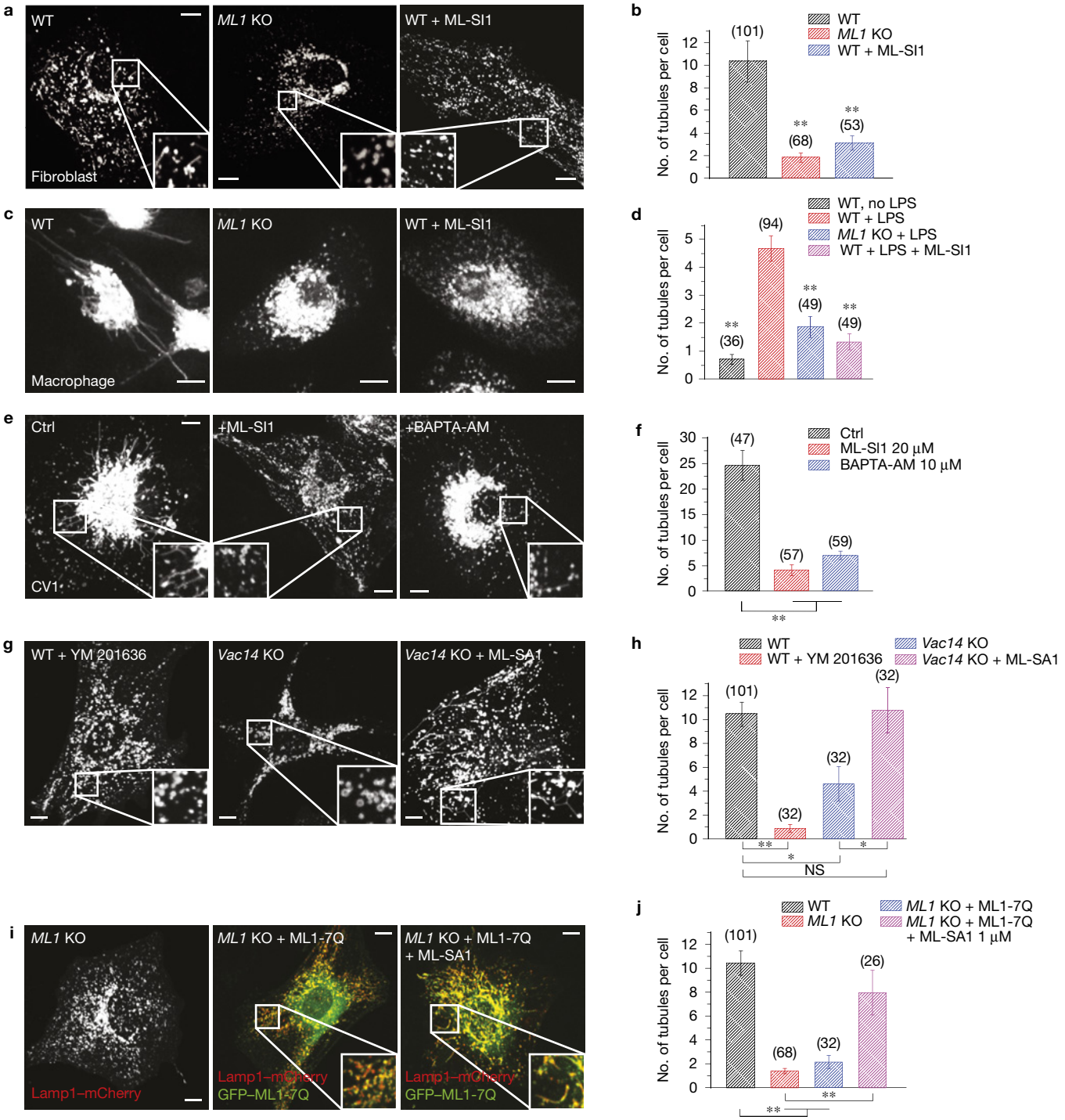

Figure 7 The PtdIns(3,5)P_2–TRPML1–Ca^{2+} pathway is required for lysosome tubulation. (**a**) Lamp1–mCherry-transfected fibroblasts were starved for 24 h. A high level of lysosome tubulation was seen in WT fibroblasts, but not in *ML1* KO fibroblasts or in WT fibroblasts treated with ML-SI1 (25 μM) during the last hour of starvation. (**b**) Quantification of the lysosome tubules in the groups shown in **a**. (**c**) Lysosome tubulation in macrophages loaded with tetramethylrhodamine–dextran (1 h loading, 2 h chase) and activated with lipopolysaccharides (LPS) for 3 h. Lysosome tubulation was prominent in WT macrophages (left), but not in *ML1* KO macrophages (middle) or WT macrophages treated with ML-SI1 (25 μM, 30 min; right). (**d**) Quantification of the groups shown in **c**. (**e**) Effects of ML-SI1 (25 μM, 1 h) or BAPTA-AM (10 μM, 1 h) on spontaneous lysosome tubulation in Lamp1–GFP-expressing CV1 cells. (**f**) Quantification of the groups shown in **e**. (**g**) Representative WT fibroblasts starved for 24 h and treated with 1 μM YM 201636 for 30 min (left), *Vac14* KO fibroblasts starved for 24 h (middle), and starved *Vac14* KO fibroblasts treated with 10 μM ML-SA1 for 30 min (right). (**h**) Quantification of the groups shown in **g**. (**i**) Lysosome tubulation after 24 h starvation of *ML1* KO fibroblasts transfected with Lamp1–mCherry alone (left), or Lamp1–mCherry together with GFP–TRPML1-7Q with (right) or without (middle) a low dose (1 μM) of ML-SA1 for 1 h. (**j**) Quantification of the groups shown in **i**. Graphed data are presented as means ± s.e.m.; the numbers of cells (*n*) used for quantification were pooled across at least three independent experiments and are shown in the parentheses. $^{*}P < 0.05$, $^{**}P < 0.01$ in ANOVA. NS, not significant. Scale bars, 10 μm.

© 2016 Macmillan Publishers Limited. All rights reserved

Supplementary Fig. 8b,c). Consistently, BAPTA-AM (ref. 54) potently inhibited lysosome tubulation in CV cells (Fig. 7e,f).

YM 201636 also potently inhibited lysosome tubulation during prolonged starvation (Fig. 7g,h). *Vac14* KO fibroblasts, which contain about half of the cellular PtdIns(3,5)P_2 found in WT cells[55], had moderately reduced lysosome tubulation. *Vac14* KO fibroblasts treated with ML-SA1 exhibited tubulation approaching that seen in WT cells (Fig. 7g,h). Furthermore, although lysosome tubulation defects in *ML1* KO fibroblasts could not be rescued with TRPML1-7Q overexpression alone (Fig. 7i,j), a low dose of ML-SA1 restored lysosome tubulation to near normal levels in TRPML1-7Q-transfected cells (Fig. 7i,j). Taken together, these data suggest that PtdIns(3,5)P_2 sensitivity of TRPML1 is required for lysosome tubulation.

TRPML1 regulates lysosome tubulation by tuning the balance between minus-end and plus-end motility

Interestingly, lysosome tubulation could be abolished by either loss of TRPML1 activity or hyper-activation of TRPML1 through TRPML1 overexpression or ML-SA1 application (Fig. 8a–c,f). We therefore reasoned that a balance between plus- and minus-end motility may be important for the generation of tubular structures on lysosomes (Fig. 8g) and that there may be an inverted-U response curve wherein too much or too little TRPML1 activity would disrupt this balance. Consistent with this hypothesis, we found that, in TRPML1-overexpressing cells, low concentrations of TRPML1 inhibitors restored lysosome tubulation (Fig. 8d,f) and high concentrations blocked lysosome tubulation (Fig. 8e,f). Likewise, in ALG-2-expressing fibroblasts, a slightly elevated degree of constitutive tubulation was observed under fed conditions, whereas lysosome tubulation was inhibited during prolonged starvation (Supplementary Fig. 8d).

DISCUSSION

The association of the microtubule-based motor proteins kinesin and dynein to lysosomes through adaptor proteins dictates the direction of lysosome movement. A series of recent studies established cholesterol as an important regulator of minus-end-directed retrograde transport of lysosomes, with the Rab7 effector RILP and the cholesterol sensor ORP1L working together to recruit the dynactin complex to the lysosome[26,29]. In this study, we report a distinct pathway through which lysosome motility is acutely regulated in an on-demand manner independent of RILP and Rab7. Whereas the cholesterol-regulated Rab7–RILP–ORP1L pathway mediates the housekeeping function of constitutive retrograde transport for endosomal maturation, the PtdIns(3,5)P_2–TRPML1–ALG-2 pathway mediates on-demand, acutely regulated transport of lysosomes towards the perinuclear region on autophagy induction.

The potential activation mechanisms of TRPML1 during starvation and autophagy induction are still an open question. PtdIns(3,5)P_2 is the only known endogenous agonist of TRPML1. Although our data showed that PtdIns(3,5)P_2 is required for retrograde transport of lysosomes, bulk cellular PtdIns(3,5)P_2 levels reportedly drop to about 40% of the control levels under acute starvation[33,56]. Therefore, PtdIns(3,5)P_2 may play only a permissive role in the process. Starvation has been shown to cause mTOR inhibition and induce cytosolic alkalization[6], and the latter is shown in the current study to directly trigger retrograde migration of lysosomes. However, TRPML1 channel activity is only slightly increased on cytosolic alkalization. mTOR was recently reported to suppress TRPML1 function through phosphorylation[57], and regulate the subcellular localization of endogenous TRPML1, as suggested by studies on *Drosophila* TRPML (ref. 58). Future studies may reveal whether mTOR inhibition plays a role in TRPML1-dependent lysosomal trafficking. However, our electrophysiology recordings do not support the possibility that TRPML1 is activated directly through mTOR inhibition. Finally, unidentified endogenous TRPML1 agonists may be produced during acute starvation and autophagy induction. Therefore, it is likely that multiple mechanisms mentioned above may be recruited to locally 'activate' TRPML1 in lysosomes on starvation and autophagy induction.

TRPML1 has been implicated in lysosomal trafficking in previous studies, and both membrane fusion and fission defects have been observed in ML-IV cells[16,59]. However, the exact role of TRPML1 in those trafficking steps is not clear as most previous studies relied on chronic inhibition of TRPML1 that causes secondary lysosome storage. Our identification of TRPML1 as a regulator in lysosome mobility prompts re-interpretation of the mechanisms underlying some previous observations. In light of the contrasting phenotypes of acute versus chronic TRPML1 inhibition on lysosome positioning, a high-priority experiment would be to verify whether acute inhibition of TRPML1 can affect previously implicated processes. Accordingly, it should be possible to distinguish between phenotypes caused by a primary loss of TRPML1 activity and those caused by chronic storage of lysosomal substances, such as cholesterol, secondary to loss of TRPML1 function.

Previously, we identified TRPML1 as a regulator of lysosome exocytosis through Ca^{2+} release[2]. The discrepancy between the function of TRPML1 in lysosome exocytosis, which happens at the cell periphery, and the retrograde transport of lysosomes towards the MTOC may be due to the involvement of different downstream Ca^{2+} effectors. Indeed, multiple downstream targets of lysosomal Ca^{2+} have been identified, including synaptotagmin-VII for lysosomal exocytosis[2], calcineurin for TFEB activation[60], and ALG-2 for lysosome motility in this study. ALG-2 has been shown to be involved in several vesicular trafficking steps, including ER-to-Golgi transport[61]. By directly interacting with the dynactin complex, ALG-2 may directly promote retrograde transport. The subcellular localization of particular lysosomes and cofactor or substrate availability may determine which Ca^{2+} effectors are activated for particular Ca^{2+} release events. For example, Ca^{2+} release from lysosomes that are docked to the plasma membrane may activate exocytosis, but not retrograde transport.

Lysosome motility is required for many lysosome functions including lysosome tubulation. Lysosome tubulation is a long-known[62], but recently characterized phenomenon that serves as a platform for lysosome reformation[4]. Under circumstances of heavy lysosome consumption, including prolonged starvation[4] and active phagocytosis[53], there is an obvious triggering of lysosome tubulation, enabling recycling of lysosomal membranes and membrane proteins and thus, replenishment of the functional lysosome pool[63]. Dysfunctions of various lysosome-related proteins have been shown to inhibit lysosome tubulation[64–66], but the mechanisms underlying these effects have not yet been delineated. Our study suggests that

© 2016 Macmillan Publishers Limited. All rights reserved

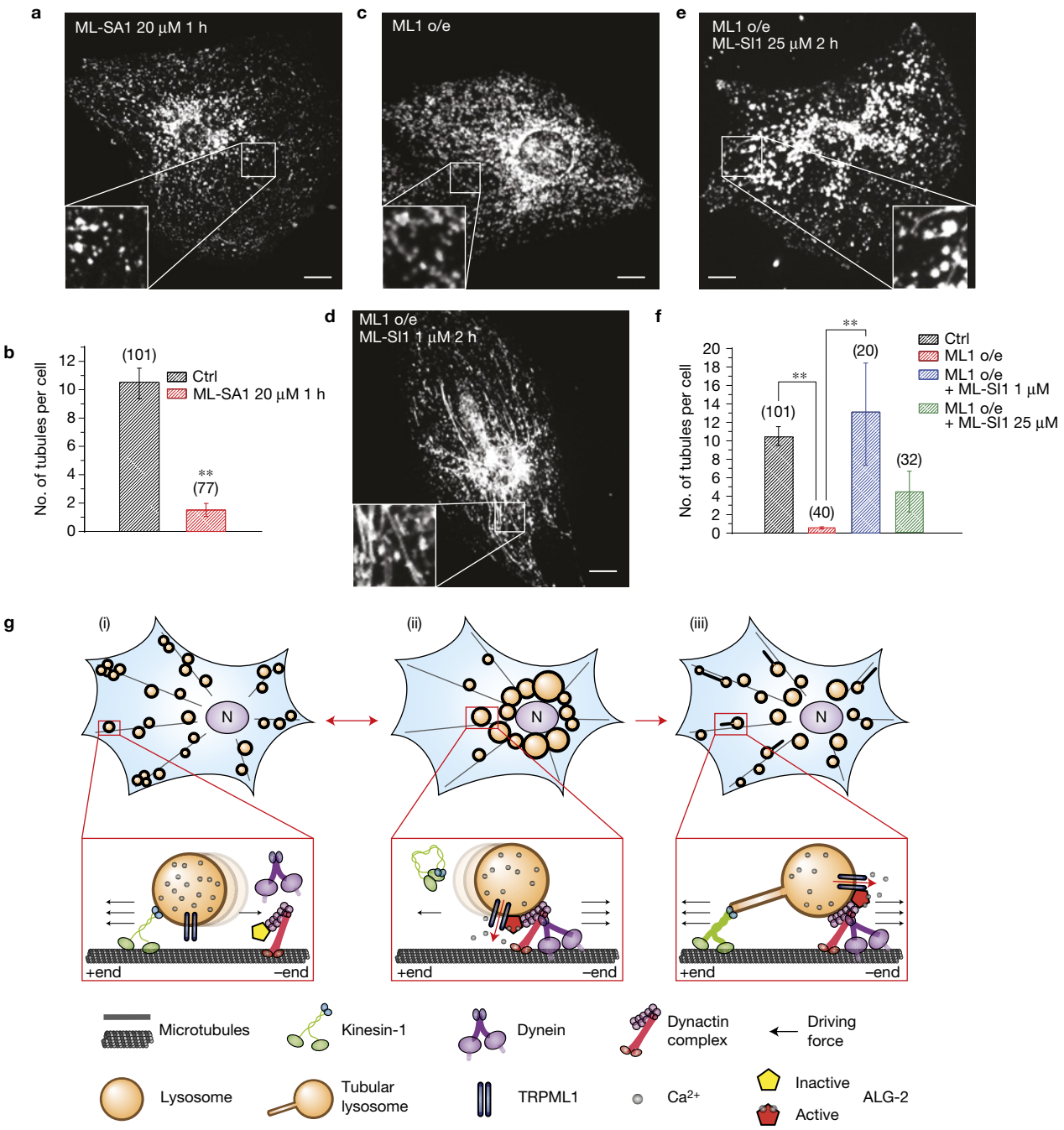

Figure 8 TRPML1 regulates the switch between the plus- and minus-end-directed lysosome motility. (**a**,**b**) Effect of ML-SA1 (20 μM, 1 h) on lysosome tubulation in mouse fibroblasts. (**c**–**e**) Effects of 1 μM (**d**) or 25 μM (**e**) ML-SI1 on lysosome tubulation in TRPML1-overexpressing WT fibroblasts. ML-SIs were applied during the last 2 h of starvation. (**f**) Quantifications of the groups shown in **c**–**e**. (**g**) Model illustrating the proposed role of TRPML1 in the regulation of lysosome motility and tubulation. Under normal growth conditions (i), lysosomes are mostly peripherally distributed. During acute starvation (ii), the TRPML1–ALG-2 pathway is activated to increase minus-end-directed motility of lysosomes, resulting in rapid redistribution of lysosomes to the juxtanuclear region, thereby facilitating autophagosome–lysosome fusion. After prolonged starvation (iii), reactivation of mTOR turns on the machinery for lysosome tubulation and reformation. While the TRPML1–ALG-2 pathway remains active, the plus-end motility of lysosomes is increased. Subsequently, the 'balanced' driving forces on both directions result in the generation of tubular lysosomes. Graphed data are presented as means ± s.e.m.; the numbers of cells (*n*) used for quantification were pooled across at least three independent experiments and are shown in the parentheses. $^{**}P < 0.01$ in ANOVA. Scale bars, 10 μm.

the dysfunctions of many of such proteins may affect tubulation through a common mechanism. A shared characteristic of most lysosome-related dysfunctions is the primary and secondary storage of substances in the lysosomes, including cholesterol. The requirement of both kinesin and dynein for lysosome tubulation suggests that tubulation processes require a balance of driving forces towards the

© 2016 Macmillan Publishers Limited. All rights reserved

two ends. Disruption of the balance will probably disrupt tubulation regardless of the circumstance under which tubulation is triggered. Cholesterol storage under such conditions may disrupt the balance of the motility, leading to the failure of generation or maintenance of tubular structures, as we demonstrated through manipulation of TRPML1 activity. Accordingly, restoration of lysosomal tubulation in disease models may be accomplished simply through fine-tuning of lysosomal motility, regardless of the nature of the dysfunction. The present findings demonstrating that TRPML1 functions as a switch in lysosomal motility regulation, together with the availability of specific TRPML1 agonists and antagonists, suggest that TRPML1 may be a valuable target for treating lysosome-related diseases. □

METHODS

Methods and any associated references are available in the online version of the paper.

Note: Supplementary Information is available in the online version of the paper

ACKNOWLEDGEMENTS

This work was supported by NIH grants (NS062792, MH096595 and AR060837 to H.X.). The authors are grateful to R. Puertollano (NHLBI, NIH, USA) for providing the mCherry–ALG-2 construct, K. Verhey (University of Michigan, USA) for providing GFP–DYNIC2-DN, GFP–dynamitin and KIF5B cDNA constructs, R. Botelho (Ryerson University, Toronto, Canada) for providing the RILP–GFP construct, J. Neefjes (Netherlands Cancer Institute, Netherlands) for providing the ORP1L–GFP construct, and D. Rubinsztein (Cambridge Institute for Medical Research, UK) for providing the LC3 stable cell line. The authors thank R. Hume, R. Fuller, K. Verhey and Y. Wang for their suggestions. We appreciate the encouragement and helpful comments from the Xu laboratory colleagues.

AUTHOR CONTRIBUTIONS

X.L. initiated the project; X.L. and H.X. designed the research; X.L., N.R., A.H., X.Z., J.Y., W.W., Q.G. and X.C. performed the experiments; X.L. generated new reagents; X.L., N.R., A.H., X.Z., J.Y., W.W., Q.G., X.C. and H.X. analysed and interpreted data; X.L. and H.X. wrote the manuscript with input from all authors.

COMPETING FINANCIAL INTERESTS

The authors declare no competing financial interests.

Published online at http://dx.doi.org/10.1038/ncb3324

Reprints and permissions information is available online at www.nature.com/reprints

1. Luzio, J. P., Pryor, P. R. & Bright, N. A. Lysosomes: fusion and function. *Nat. Rev. Mol. Cell Biol.* **8,** 622–632 (2007).
2. Samie, M. A. & Xu, H. Lysosomal exocytosis and lipid storage disorders. *J. Lipid Res.* **55,** 995–1009 (2014).
3. Samie, M. *et al.* A TRP channel in the lysosome regulates large particle phagocytosis via focal exocytosis. *Dev. Cell* **26,** 511–524 (2013).
4. Yu, L. *et al.* Termination of autophagy and reformation of lysosomes regulated by mTOR. *Nature* **465,** 942–946 (2010).
5. Akhmanova, A. & Hammer, J. A. 3rd Linking molecular motors to membrane cargo. *Curr. Opin. Cell Biol.* **22,** 479–487 (2010).
6. Korolchuk, V. I. *et al.* Lysosomal positioning coordinates cellular nutrient responses. *Nat. Cell Biol.* **13,** 453–460 (2011).
7. Hirokawa, N. Kinesin and dynein superfamily proteins and the mechanism of organelle transport. *Science* **279,** 519–526 (1998).
8. King, S. M. The dynein microtubule motor. *Biochim. Biophys. Acta* **1496,** 60–75 (2000).
9. Schwarz, T. L. Mitochondrial trafficking in neurons. *Cold Spring Harb. Perspect. Biol.* **5,** a011304 (2013).
10. Dong, X. P. *et al.* The type IV mucolipidosis-associated protein TRPML1 is an endolysosomal iron release channel. *Nature* **455,** 992–996 (2008).
11. Cheng, X., Shen, D., Samie, M. & Xu, H. Mucolipins: intracellular TRPML1-3 channels. *FEBS Lett.* **584,** 2013–2021 (2010).
12. Bassi, M. T. *et al.* Cloning of the gene encoding a novel integral membrane protein, mucolipidin-and identification of the two major founder mutations causing mucolipidosis type IV. *Am. J. Human Genet.* **67,** 1110–1120 (2000).
13. Chen, C. S., Bach, G. & Pagano, R. E. Abnormal transport along the lysosomal pathway in mucolipidosis, type IV disease. *Proc. Natl Acad. Sci. USA* **95,** 6373–6378 (1998).
14. Venugopal, B. *et al.* Neurologic, gastric, and opthalmologic pathologies in a murine model of mucolipidosis type IV. *Am. J. Human Genet.* **81,** 1070–1083 (2007).
15. Dayam, R. M., Saric, A., Shilliday, R. E. & Botelho, R. J. The phosphoinositide-gated lysosomal Ca(2+) channel, TRPML1, is required for phagosome maturation. *Traffic* **16,** 1010–1026 (2015).
16. Xu, H. & Ren, D. Lysosomal physiology. *Annu. Rev. Physiol.* **77,** 57–80 (2015).
17. Xu, M. *et al.* Regulation of autophagic flux by dynein-mediated autophagosomes trafficking in mouse coronary arterial myocytes. *Biochim. Biophys. Acta* **1833,** 3228–3236 (2013).
18. Kimura, S., Noda, T. & Yoshimori, T. Dynein-dependent movement of autophagosomes mediates efficient encounters with lysosomes. *Cell Struct. Funct.* **33,** 109–122 (2008).
19. Thoreen, C. C. *et al.* An ATP-competitive mammalian target of rapamycin inhibitor reveals rapamycin-resistant functions of mTORC1. *J. Biol. Chem.* **284,** 8023–8032 (2009).
20. Curcio-Morelli, C. *et al.* Macroautophagy is defective in mucolipin-1-deficient mouse neurons. *Neurobiol. Dis.* **40,** 370–377 (2010).
21. Vergarajauregui, S., Connelly, P. S., Daniels, M. P. & Puertollano, R. Autophagic dysfunction in mucolipidosis type IV patients. *Human Mol. Genet.* **17,** 2723–2737 (2008).
22. Cheng, X. *et al.* The intracellular Ca channel MCOLN1 is required for sarcolemma repair to prevent muscular dystrophy. *Nat. Med.* **20,** 1187–1192 (2014).
23. Wang, W. *et al.* Up-regulation of lysosomal TRPML1 channels is essential for lysosomal adaptation to nutrient starvation. *Proc. Natl Acad. Sci. USA* **112,** E1373–E1381 (2015).
24. Shen, D. *et al.* Lipid storage disorders block lysosomal trafficking by inhibiting a TRP channel and lysosomal calcium release. *Nat. Commun.* **3,** 731 (2012).
25. Chen, H., Yang, J., Low, P. S. & Cheng, J. X. Cholesterol level regulates endosome motility via Rab proteins. *Biophys. J.* **94,** 1508–1520 (2008).
26. Rocha, N. *et al.* Cholesterol sensor ORP1L contacts the ER protein VAP to control Rab7-RILP-p150 Glued and late endosome positioning. *J. Cell Biol.* **185,** 1209–1225 (2009).
27. Kwiatkowska, K. *et al.* Visualization of cholesterol deposits in lysosomes of Niemann-Pick type C fibroblasts using recombinant perfringolysin O. *Orphanet J. Rare Dis.* **9,** 64 (2014).
28. Reid, P. C., Sugii, S. & Chang, T. Y. Trafficking defects in endogenously synthesized cholesterol in fibroblasts, macrophages, hepatocytes, and glial cells from Niemann-Pick type C1 mice. *J. Lipid Res.* **44,** 1010–1019 (2003).
29. Schroer, T. A. Dynactin. *Annu. Rev. Cell Dev. Biol.* **20,** 759–779 (2004).
30. Spinosa, M. R. *et al.* Functional characterization of Rab7 mutant proteins associated with Charcot-Marie-Tooth type 2B disease. *J. Neurosci.* **28,** 1640–1648 (2008).
31. Cantalupo, G., Alifano, P., Roberti, V., Bruni, C. B. & Bucci, C. Rab-interacting lysosomal protein (RILP): the Rab7 effector required for transport to lysosomes. *EMBO J.* **20,** 683–693 (2001).
32. Bucci, C., Thomsen, P., Nicoziani, P., McCarthy, J. & vanDeurs, B. Rab7: a key to lysosome biogenesis. *Mol. Biol. Cell* **11,** 467–480 (2000).
33. Li, X. *et al.* Genetically encoded fluorescent probe to visualize intracellular phosphatidylinositol 3,5-bisphosphate localization and dynamics. *Proc. Natl Acad. Sci. USA* **110,** 21165–21170 (2013).
34. Vicinanza, M. *et al.* PI(5)P regulates autophagosome biogenesis. *Mol. Cell* **57,** 219–234 (2015).
35. Dong, X. P. *et al.* PI(3,5)P(2) controls membrane trafficking by direct activation of mucolipin Ca^{2+} release channels in the endolysosome. *Nat. Commun.* **1,** 38 (2010).
36. Zhang, X., Li, X. & Xu, H. Phosphoinositide isoforms determine compartment-specific ion channel activity. *Proc. Natl Acad. Sci. USA* **109,** 11384–11389 (2012).
37. Jefferies, H. B. *et al.* A selective PIKfyve inhibitor blocks $PtdIns(3,5)P_2$ production and disrupts endomembrane transport and retroviral budding. *EMBO Rep.* **9,** 164–170 (2008).
38. Martin, S. *et al.* Inhibition of PIKfyve by YM-201636 dysregulates autophagy and leads to apoptosis-independent neuronal cell death. *PLoS ONE* **8,** e60152 (2013).
39. Ho, C. Y., Choy, C. H., Wattson, C. A., Johnson, D. E. & Botelho, R. J. The Fab1/PIKfyve phosphoinositide phosphate kinase is not necessary to maintain the pH of lysosomes and of the yeast vacuole. *J. Biol. Chem.* **290,** 9919–9928 (2015).
40. Cai, X. *et al.* PIKfyve, a class III PI kinase, is the target of the small molecular IL-12/IL-23 inhibitor apilimod and a player in Toll-like receptor signaling. *Chem. Biol.* **20,** 912–921 (2013).
41. Verhey, K. J. & Hammond, J. W. Traffic control: regulation of kinesin motors. *Nat. Rev. Mol. Cell Biol.* **10,** 765–777 (2009).
42. Rosa-Ferreira, C. & Munro, S. Arl8 and SKIP act together to link lysosomes to kinesin-1. *Dev. Cell* **21,** 1171–1178 (2011).
43. Tanaka, Y. *et al.* Targeted disruption of mouse conventional kinesin heavy chain, kif5B, results in abnormal perinuclear clustering of mitochondria. *Cell* **93,** 1147–1158 (1998).
44. Jordens, I. *et al.* The Rab7 effector protein RILP controls lysosomal transport by inducing the recruitment of dynein-dynactin motors. *Curr. Biol.* **11,** 1680–1685 (2001).
45. Johansson, M. *et al.* Activation of endosomal dynein motors by stepwise assembly of Rab7-RILP-p150Glued, ORP1L, and the receptor betalII spectrin. *J. Cell Biol.* **176,** 459–471 (2007).
46. Silver, K. E. & Harrison, R. E. Kinesin 5B is necessary for delivery of membrane and receptors during FcgammaR-mediated phagocytosis. *J. Immunol.* **186,** 816–825 (2011).
47. King, S. J., Brown, C. L., Maier, K. C., Quintyne, N. J. & Schroer, T. A. Analysis of the dynein-dynactin interaction *in vitro* and *in vivo*. *Mol. Biol. Cell* **14,** 5089–5097 (2003).

© 2016 Macmillan Publishers Limited. All rights reserved

48. Sainath, R. & Gallo, G. The dynein inhibitor Ciliobrevin D inhibits the bidirectional transport of organelles along sensory axons and impairs NGF-mediated regulation of growth cones and axon branches. *Dev. Neurobiol.* **75,** 757–777 (2014).
49. Firestone, A. J. *et al.* Small-molecule inhibitors of the AAA+ ATPase motor cytoplasmic dynein. *Nature* **484,** 125–129 (2012).
50. Maki, M., Suzuki, H. & Shibata, H. Structure and function of ALG-2, a penta-EF-hand calcium-dependent adaptor protein. *Sci. China Life Sci.* **54,** 770–779 (2011).
51. Vergarajauregui, S., Martina, J. A. & Puertollano, R. Identification of the penta-EF-hand protein ALG-2 as a Ca^{2+}-dependent interactor of mucolipin-1. *J. Biol. Chem.* **284,** 36357–36366 (2009).
52. Cong, L. & Zhang, F. Genome engineering using CRISPR-Cas9 system. *Methods Mol. Biol.* **1239,** 197–217 (2015).
53. Mrakovic, A., Kay, J. G., Furuya, W., Brumell, J. H. & Botelho, R. J. Rab7 and Arl8 GTPases are necessary for lysosome tubulation in macrophages. *Traffic* **13,** 1667–1679 (2012).
54. Tsien, R. Y. New calcium indicators and buffers with high selectivity against magnesium and protons: design, synthesis, and properties of prototype structures. *Biochemistry* **19,** 2396–2404 (1980).
55. Jin, N. *et al.* VAC14 nucleates a protein complex essential for the acute interconversion of PI3P and PI(3,5)P(2) in yeast and mouse. *EMBO J.* **27,** 3221–3234 (2008).
56. Zolov, S. N. *et al. In vivo*, Pikfyve generates PI(3,5)P2, which serves as both a signaling lipid and the major precursor for PI5P. *Proc. Natl Acad. Sci. USA* **109,** 17472–17477 (2012).
57. Onyenwoke, R. U. *et al.* The mucolipidosis IV Ca^{2+} channel TRPML1 (MCOLN1) is regulated by the TOR kinase. *Biochem. J.* **470,** 331–342 (2015).
58. Wong, C. O., Li, R., Montell, C. & Venkatachalam, K. *Drosophila* TRPML is required for TORC1 activation. *Curr. Biol.* **22,** 1616–1621 (2012).
59. Miller, A. *et al.* Mucolipidosis type IV protein TRPML1-dependent lysosome formation. *Traffic* **16,** 284–297 (2014).
60. Medina, D. L. *et al.* Lysosomal calcium signalling regulates autophagy through calcineurin and TFEB. *Nat. Cell Biol.* **17,** 288–299 (2015).
61. Helm, J. R. *et al.* Apoptosis-linked gene-2 (ALG-2)/Sec31 interactions regulate endoplasmic reticulum (ER)-to-Golgi transport: a potential effector pathway for luminal calcium. *J. Biol. Chem.* **289,** 23609–23628 (2014).
62. Swanson, J., Bushnell, A. & Silverstein, S. C. Tubular lysosome morphology and distribution within macrophages depend on the integrity of cytoplasmic microtubules. *Proc. Natl Acad. Sci. USA* **84,** 1921–1925 (1987).
63. Chen, Y. & Yu, L. Autophagic lysosome reformation. *Exp. Cell Res.* **319,** 142–146 (2013).
64. Rong, Y. *et al.* Clathrin and phosphatidylinositol-4,5-bisphosphate regulate autophagic lysosome reformation. *Nat. Cell Biol.* **14,** 924–934 (2012).
65. Rong, Y. *et al.* Spinster is required for autophagic lysosome reformation and mTOR reactivation following starvation. *Proc. Natl Acad. Sci. USA* **108,** 7826–7831 (2011).
66. Chang, J., Lee, S. & Blackstone, C. Spastic paraplegia proteins spastizin and spatacsin mediate autophagic lysosome reformation. *J. Clin. Invest.* **124,** 5249–5262 (2014).

© 2016 Macmillan Publishers Limited. All rights reserved

METHODS

DNA subcloning. GFP–TRPML1, GFP–TRPML1-7Q, Lamp1–GFP and Lamp1–mCherry constructs were generated as described previously[33]. Dominant-negative KIF5B (human KIF5B amino acid residues 592–963) was subcloned to pmCherry–C1 (Clontech) using KIF5B cDNA as the template. Dominant-negative dynein intermediate chain 2 (GFP–DYNIC2-DN) and GFP–dynamitin (both gifts from K. Verhey, University of Michigan, USA) have been characterized previously[47,67]. mCherry–ALG-2 and GFP–TRPML1-R^{44}LK-AAA were provided by R. Puertollano (NHLBI, NIH, USA). mCherry–ALG-2-$E^{47}E^{114}$-AA, GFP–TRPML1-R^{44}-A, GFP–TRPML1-L^{45}-A, Rab7-T^{22}N–GFP and Rab7-Q^{67}L–GFP mutants were generated with a site-directed mutagenesis kit. All constructs were verified with sequencing and confirmed with western blotting.

Mouse lines. Characterizations of *TRPML1* (ref. 14), *NPC1* and *Vac14* (ref. 55) KO mice were performed as described previously. Animals were used under approved animal protocols and the Institutional Animal Care Guidelines of the University of Michigan.

Generation of *ALG-2* KO HeLa cells using CRISPR/Cas9. An SpCas9 plasmid was obtained from Addgene (no. 48139). Primers for guide RNA generation are as follows: no. 1 forward: 5′-CACCGAGGGCCGGGGCGGTAAGAGT-3′; no. 1 reverse: 5′-AAACACTCTTACCGCCCCGGCCCTC-3′; no. 2 forward: 5′-CACCG CTCTTACCGCCCCGGCCCTG-3′; no. 2 reverse: 5′-AAACCAGGGCCGGGGCG GTAAGAGC-3′.

ALG-2 KO HeLa cells were generated using protocols established previously[52]. Briefly, primers were annealed and incorporated onto the plasmid using the BpiI site. WT HeLa cells were transfected with the plasmid and followed by a 2-day puromycin selection after transfection for 24 h. The cells were then plated on 96-well plates with an average density of 0.5 cell per well. Single colonies were selected and sequenced. Identified mutant lines were confirmed by western blotting using anti-ALG-2.

Mammalian cell culture and transfection. Mammalian cells were cultured in a 37 °C, 5% CO_2 incubator. Mouse fibroblasts[35] and macrophages[3] were isolated and cultured as previously described. Immortalized cell lines (Cos1, HEK293, HeLa, CV-1, NRK) were originated from ATCC and cultured following standard tissue culture protocols, but were not tested for mycoplasma contamination. HEK293 cells are on the list of frequently misidentified or cross-contaminated cell lines, but were used only in the co-immunoprecipitation experiments with endogenous proteins owing to antibody specificity. All other cell types used in the study are not listed as misidentified or cross-contaminated cells. Unless otherwise indicated, all cells were cultured in Dulbecco's modified Eagle medium (DMEM; Invitrogen) supplemented with 10% fetal bovine serum (FBS; Gemini). Macrophages were further supplemented with murine GM-CSF (Peprotech). For macrophages, dextran red (0.5 mg ml^{-1}) was used to visualize lysosomes using a protocol of 1 h loading followed by 2 h of chasing. For fibroblasts, transfection was performed using the Neon electroporation kit (Invitrogen). All other cell types were transfected with Lipofectamine 2000 (Invitrogen). Culture media were refreshed 18–24 h post-transfection, and cells were imaged 48 h post-transfection to allow sufficient recovery from transfection stress. Note that unlike non-transfected cells, lysosomes in transfected cells exhibited a perinuclear localization pattern within 24 h of transfection, probably because of cell stress. For starvation, complete medium was replaced with DMEM without supplements through careful and extensive washes.

Ammonia Ringer's solution. Ammonia Ringer was adapted from that of acidic Ringer's solution[33,68] and contained (in mM) 130 HCl, 20 NH_4Cl, 5 KCl, 2 $CaCl_2$, 1 $MgCl_2$, 2 NaH_2PO_4, 10 HEPES, and 10 glucose; after mixing, the solution was adjusted to a pH of 7.9 with NaOH.

Immunolabelling. Lamp1–GFP-transfected cells were rinsed with phosphate-buffered saline (PBS) and fixed in 4% paraformaldehyde for 20 min at room temperature. Fixed cells were washed and blocked with 2% bovine serum albumin in PBS for 2 h, and then incubated overnight with primary antibodies in the blocking solution. Cells were then washed and incubated with secondary antibodies for 1 h before being subjected to fluorescent imaging.

Filipin staining and quantification. Filipin staining was performed as described previously[23]. Briefly, filipin was dissolved in dimethylsulphoxide at 25 mg ml^{-1} as a stock solution. The cells were incubated with filipin working solution (0.05 mg ml^{-1}) at room temperature for 2 h, and washed with PBS four times before imaging. All manipulations involving Filipin were kept strictly in the dark until imaging. ImageJ was used to analyse the staining results. For each individual cell, the fluorescence intensities of three randomly selected areas close to the cell border were averaged, subtracted with the image background noise (intensity of void areas), then multiplied by the cell area, and considered intracellular background intensity. Note that because lysosomes are the primary storage sites of unesterified cholesterol under cholesterol storage conditions (see Fig. 3), the puncta filipin signal was presumed to be originated from lysosomal cholesterol[69]. Lysosomal cholesterol was then normalized as 100× lysosomal intensity/intracellular background intensity.

Cholesterol depletion. Depletion of cholesterol was performed as described previously[26]. Briefly, 50 μM of activated simvastatin was applied to DMEM without FBS, and then supplemented with 230 μM mevalonate (to supply essential non-sterol isoprenoids) in the absence of cholesterol[26]. Cells were washed extensively and incubated in the cholesterol-depleting medium for 3 h before imaging.

Fluorescence imaging and image analysis. Live imaging was performed with an Olympus spinning-disc confocal microscope equipped with a heated chamber to maintain the specimen temperature at ∼37 °C. Except for FRAP experiments, which were carried out using a 3 × 1 μm z-stack setting for fast speed, all live imaging was carried out using a 0.3 μm step size z-stack setting from the top to the bottom of the cells. GFP-tagged proteins were visualized with a 488/515 (excitation/emission in nanometres) filter set; mCherry-tagged proteins were visualized with a 561/607 filter set. Quantification was performed in ImageJ.

Photobleaching and quantification of lysosome movement. Photobleaching experiments were performed with the FRAP function of Metamorph software in an Olympus spinning-disc confocal system. Briefly, after cells were incubated at ∼37 °C for 10 min, a region (10 μm × 25–30 μm, corresponding to 42 pixels × 106–127 pixels at 60× magnification) was selected for photobleaching with an 800 ms per pulse protocol (561 nm excitation), and then live-imaged for 5 min (1 frame s^{-1}) with a z-stack of three 1-μm steps using a 561/607 filter set. The midline of each bleached area was drawn, and the number of lysosomes crossing the midline in each direction during the 5-min imaging time was counted.

Co-immunoprecipitation. Transfected cells from 10 cm dishes were incubated with 1 ml of lysis buffer (1% NP-40, 0.25% Na-deoxycholate, 1 mM Na_3VO_4, 1 mM NaF, 150 mM NaCl, 0.5 mM $CaCl_2$ in 50 mM Tris-HCl, adjusted to pH 7.4) for 30 min at 4 °C. Lysates were centrifuged at 16,000g for 10 min, and supernatants were incubated with 3 μg of primary antibodies at 4 °C for 1 h. After addition of 30 μl of protein A/G plus-agarose, lysates were incubated at 4 °C overnight with gentle shaking. Agarose beads were then collected through centrifugation at 500g for 5 min. Beads were washed four times in lysis buffer, and then heated to 60 °C for 10 min in NuPAGE loading buffer. Proteins were blotted with anti-GFP, anti-mCherry (1:5,000), or anti-dynamitin (1:1,000).

Quantification of lysosome distribution. Lysosome distribution was analysed in fibroblasts with cell areas in the range of 2,500–7,500 μm^2, and in HeLa cells ranging 800–2,500 μm^2. The nuclear area was excluded during quantification. Average Lamp1 intensities were measured for the whole cell (I_{total}), the area within 10 μm of the nucleus ($I_{perinuclear}$), and the area >15 μm from the nucleus ($I_{peripheral}$). For HeLa cells, the last two areas were within 5–10 μm of the nucleus, respectively. The perinuclear and peripheral normalized intensities were first calculated and normalized as $I_{<10} = I_{perinuclear}/I_{total} - 100$ and $I_{>15} = I_{peripheral}/I_{total} - 100$, respectively ($I_{<5}$ and $I_{>10}$ for HeLa cells). The perinuclear index was defined as $I_{<10} - I_{>15}$ ($I_{<5} - I_{>10}$ for HeLa cells). Quantifications were done by researchers blind to the experimental groups presented.

Quantification of lysosome tubulation. Cells were chosen randomly with the criterion that their fluorescence was strong enough to visualize tubular structures. Only tubules longer than 2 μm were included in the analysis to reduce false-positive hits (see Supplementary Fig. 8e,f). Quantifications were done by researchers blind to the experimental groups presented.

Endolysosomal electrophysiology. Endolysosomal electrophysiology was performed in isolated enlarged endolysosomes with a modified patch-clamp method as described previously[24,35,36,70]. The pipette (luminal) solution was modified Tyrode's, including (in mM) 145 NaCl, 5 KCl, 2 $CaCl_2$, 1 $MgCl_2$, 10 HEPES, 10 MES, 10 glucose (pH adjusted with NaOH to pH 4.6). The bath (internal/cytoplasmic) solution contained (in mM) 140 K-gluconate, 4 NaCl, 1 EGTA, 2 $MgCl_2$, 0.39 $CaCl_2$, 20 HEPES (pH adjusted with KOH to 7.2; free $[Ca^{2+}]_i \sim 100$ nM estimated using MaxChelator software). Data were collected using an Axopatch 2A patch-clamp amplifier, Digidata 1440, and pClamp 10.2 software (Axon Instruments). All recordings were analysed with pClamp 10.2, and Origin 8.0 (OriginLab).

Chemicals and reagents. Chemicals were obtained from the following vendors: ML-SA1 (Princeton BioMolecular Research), simvastatin (Sigma), PtdIns(3,5)P_2 (Echelon), ML-SI3 (AKOS), BAPTA-AM (Invitrogen), YM 201636 (Symansis), and

© 2016 Macmillan Publishers Limited. All rights reserved

DOI: 10.1038/ncb3324

ciliobrevin D (EMD Millipore). Antibodies were purchased from Sigma (γ-tubulin, T5326, clone GTU-88, used at 1:500), BD Biosciences (dynamitin, 611002, clone 25/dynactin p50, 1:250 for pulldown, and 1:1,000 for western blot), Invitrogen (GFP, A11121, clone 11E5, 1:250 for pulldown, and 1:5,000 for western blot), and Novus Biologicals (ALG-2, H00010016-M01, clone 2B4, 1:500 for western blot; mCherry, NBP1-96752, clone 1C51, 1:250 for pulldown, and 1:5,000 for western blot).

Statistics and reproducibility. Statistical data are presented as means ± standard error of the mean (s.e.m.). Comparisons between the experimental groups were made using analyses of variance (ANOVAs). All data are generated from cells pooled from at least three biologically independent experiments, with the actual sample size (*n*) shown on top of each bar in the graphs. No sample was excluded.

67. Burkhardt, J. K., Echeverri, C. J., Nilsson, T. & Vallee, R. B. Overexpression of the dynamitin (p50) subunit of the dynactin complex disrupts dynein-dependent maintenance of membrane organelle distribution. *J. Cell Biol.* **139,** 469–484 (1997).
68. Durchfort, N. *et al.* The enlarged lysosomes in *beige*$_j$ cells result from decreased lysosome fission and not increased lysosome fusion. *Traffic* **13,** 108–119 (2012).
69. Chu, B. B. *et al.* Cholesterol transport through lysosome-peroxisome membrane contacts. *Cell* **161,** 291–306 (2015).
70. Wang, X. *et al.* TPC proteins are phosphoinositide-activated sodium-selective ion channels in endosomes and lysosomes. *Cell* **151,** 372–383 (2012).

© 2016 Macmillan Publishers Limited. All rights reserved

nature cell biology

DOI: 10.1038/ncb3324

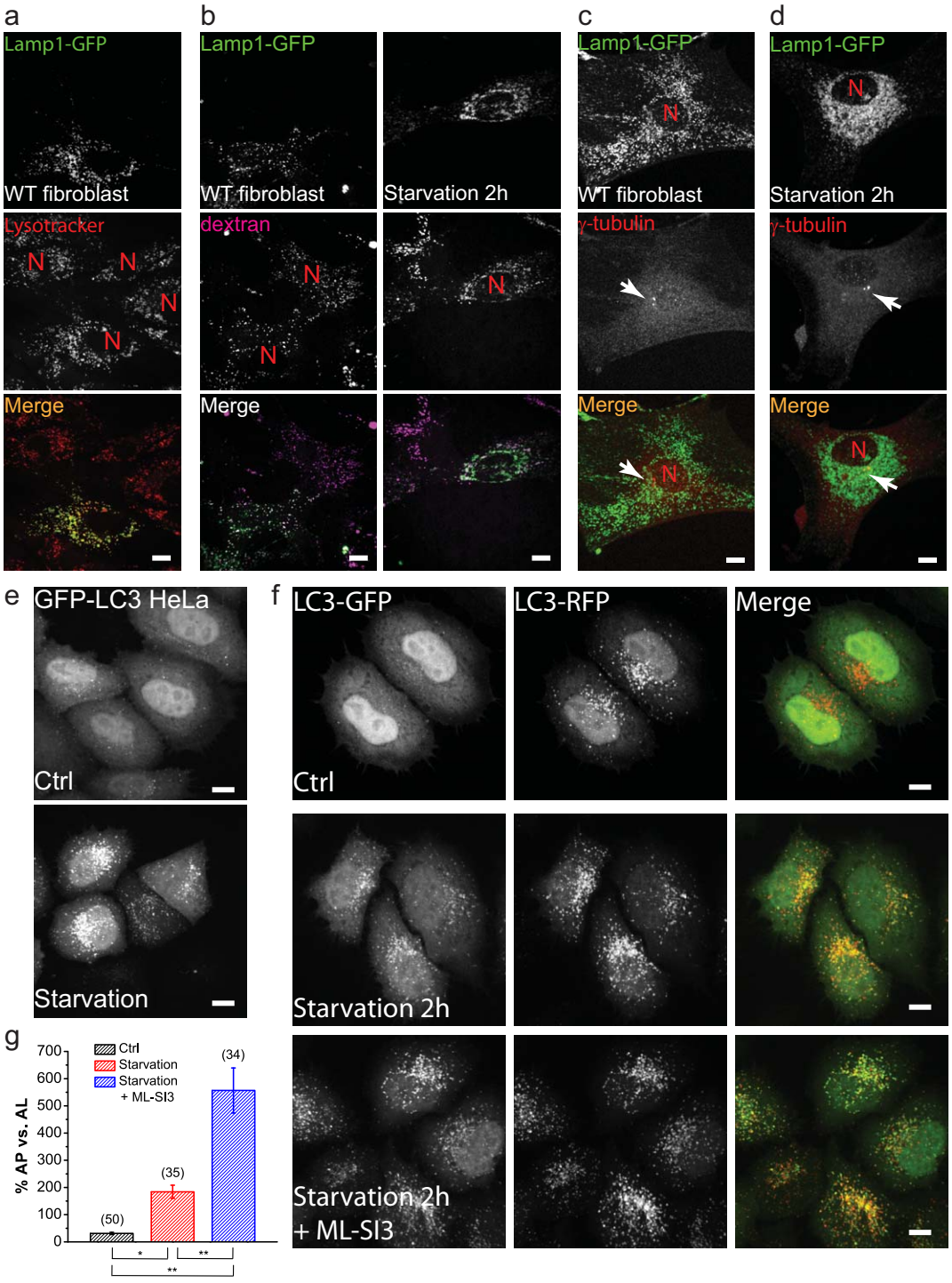

Supplementary Figure 1 Lysosomes undergo perinuclear migration during acute starvation to facilitate lysosome-autophagosome fusion. (**a**) WT fibroblasts showing the co-localization between Lamp1-GFP and Lyso-Tracker. (**b**) Lamp1-transfected WT fibroblasts were loaded with dextran-red, with (right) or without (left) starvation. (**c, d**) WT fibroblasts were transfected with Lamp1-GFP and left untreated (**c**), or starved for 2 h (**d**), then fixed and immunolabelled for γ-tubulin to visualize centrosomes (MTOC, white arrows). (**e**) HeLa cells stably expressing GFP-RFP-LC3 were subjected to starvation for 2 h (lower panel). The GFP channel shows puncta that label autophagosomes specifically, but not autolysosomes. These results show that both lysosomes and autophagosomes are perinuclearly localized under acute starvation. (**f**) HeLa cells stably expressing GFP-RFP-LC3 were left untreated (upper), starved for 2 h (middle), or starved for 2 h in the presence of 25 μM ML-SI3 (bottom). (**g**) Quantification of the number of puncta that were GFP- and RFP-positive (autophagosomes, AP) over the number of puncta that were only RFP-positive (autolysosomes, AL) for groups shown in (**f**). Nuclei are labeled with "N". Graphed data are presented as means ± SEM, the numbers of cells (n) used for quantification were pooled across at least three independent experiments and are shown in the parenthese.s $*p < .05$, $**p < .01$ in ANOVA. Scale bar = 10 μm.

© 2016 Macmillan Publishers Limited. All rights reserved

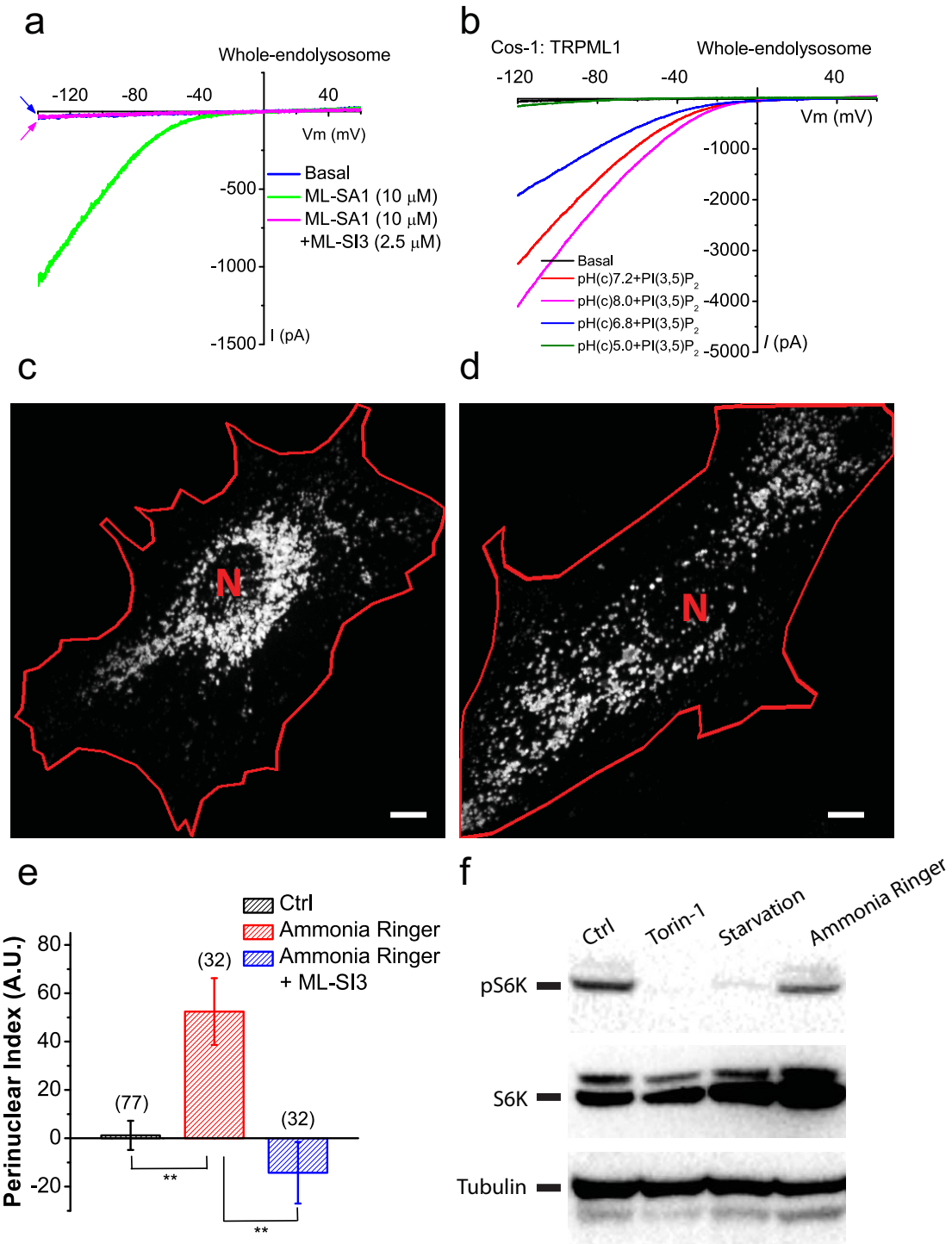

Supplementary Figure 2 Effect of cytosolic pH on TRPML1 channel activity and lysosome positioning. (**a**) ML-SA1 (10 μM)-activated whole-lysosome TRPML1 currents were inhibited potently by the TRPML1 inhibitor ML-SI3 (2.5 μM). (**b**) $PI(3,5)P_2$-activated whole-endolysosome TRPML1 currents were modulated by cytosolic pH. (**c, d**) Lamp1-mCherry-transfected WT fibroblasts were treated with 30 min ammonia Ringer's solution in the presence (**d**) or absence (**c**) of 25 μM ML-SI3. (**e**) Quantification of groups shown in (**c**) and (**d**). (**f**) Western blot showing the phosphorylated form of S6K (pS6K) in HeLa cells starved for 2 h, treated with 1 μM Torin-1 for 2 h, or treated with ammonia Ringer's for 30 min. Red lines outline cell boundaries and nuclei are marked with a red "N". Graphed data are presented as means ± SEM, the numbers of cells (n) used for quantification were pooled across at least three independent experiments and are shown in the parentheses.*$p < .05$, **$p < .01$ in ANOVA. Scale bars = 10 μm. Uncropped western blot images are shown in Supplementary Figure 9.

© 2016 Macmillan Publishers Limited. All rights reserved

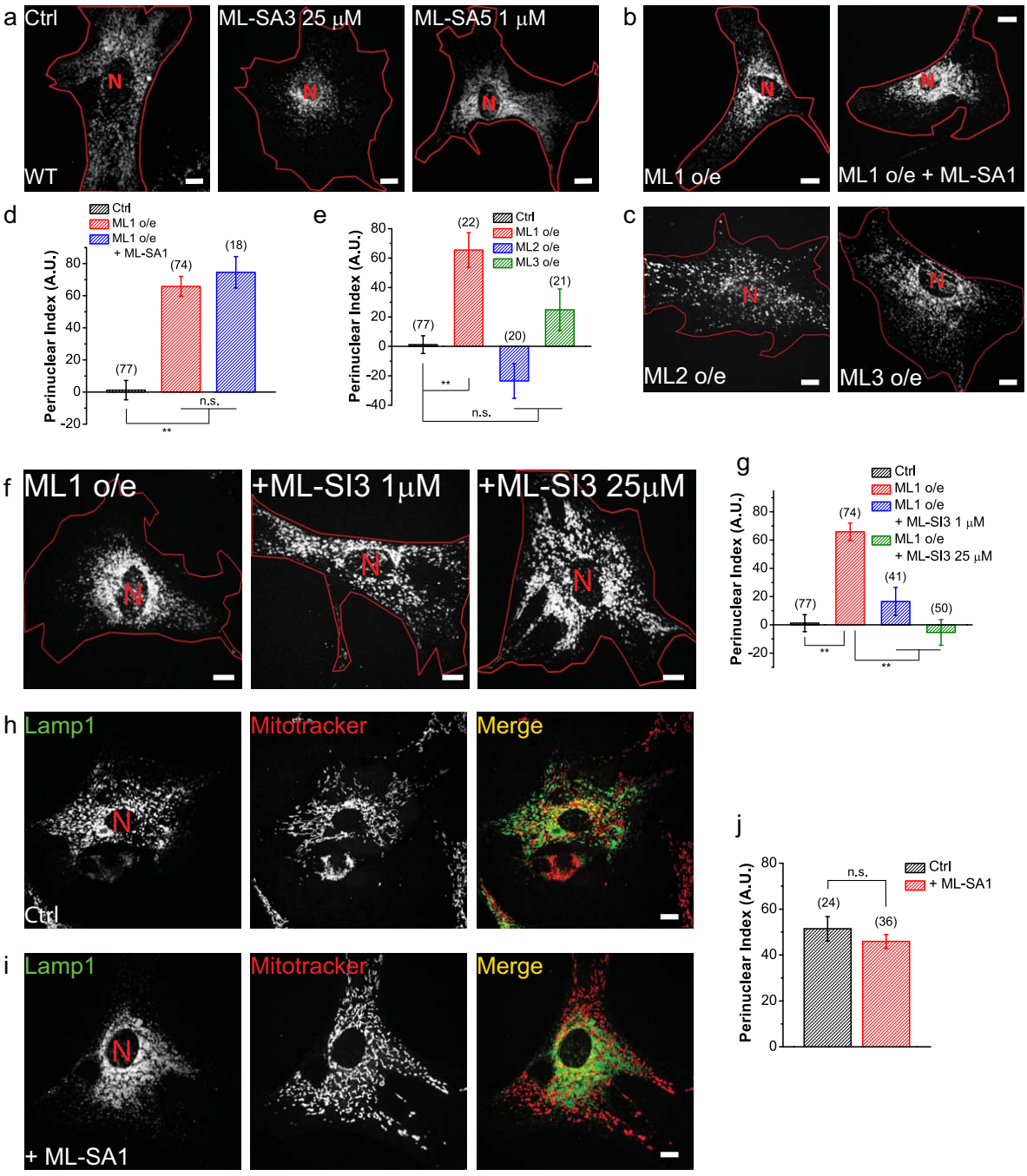

Supplementary Figure 3 Specific regulation of lysosome distribution by TRPML1. (**a**) WT fibroblasts treated with ML-SA3 (25 μM) or ML-SA5 (1 μM), two structurally-independent TRPML1 agonists, for 1 h. (**b**) In TRPML1-overexpressing cells, the majority of lysosomes were localized in the perinuclear region in the presence or absence of 25 μM ML-SA1. (**c**) Representative images showing WT fibroblasts overexpressing TRPML2 or TRPML3. (**d**) Quantifications of groups shown in (**b**). (**e**) Quantification of groups shown in (**c**). (**f**) The perinuclear localization of lysosomes induced by TRPML1 overexpression (left) was reversed by either a low (1 μM, middle) or high (25 μM, right) dose of ML-SI3. (**g**) Quantification of groups shown in (**f**). (**h, i**) Representative images of Lamp1-GFP-transfected fibroblasts stained with MitoTracker (100 nM) for 1 h (**h**), or 1 h of MitoTracker in the presence of 25 μM ML-SA1 (**i**). (**j**) Quantification of groups shown in (**h**) and (**i**). Upon ML-SA1 treatment, lysosomes became more perinuclear, while the distribution of mitochondria was not altered. Red lines outline cell boundaries and nuclei are marked with a red "N". Graphed data are presented as means ± SEM, the numbers of cells (n) used for quantification were pooled across at least three independent experiments and are shown in the parentheses $*p < .05$, $**p < .01$ in ANOVA. Scale bars = 10 μm.

© 2016 Macmillan Publishers Limited. All rights reserved

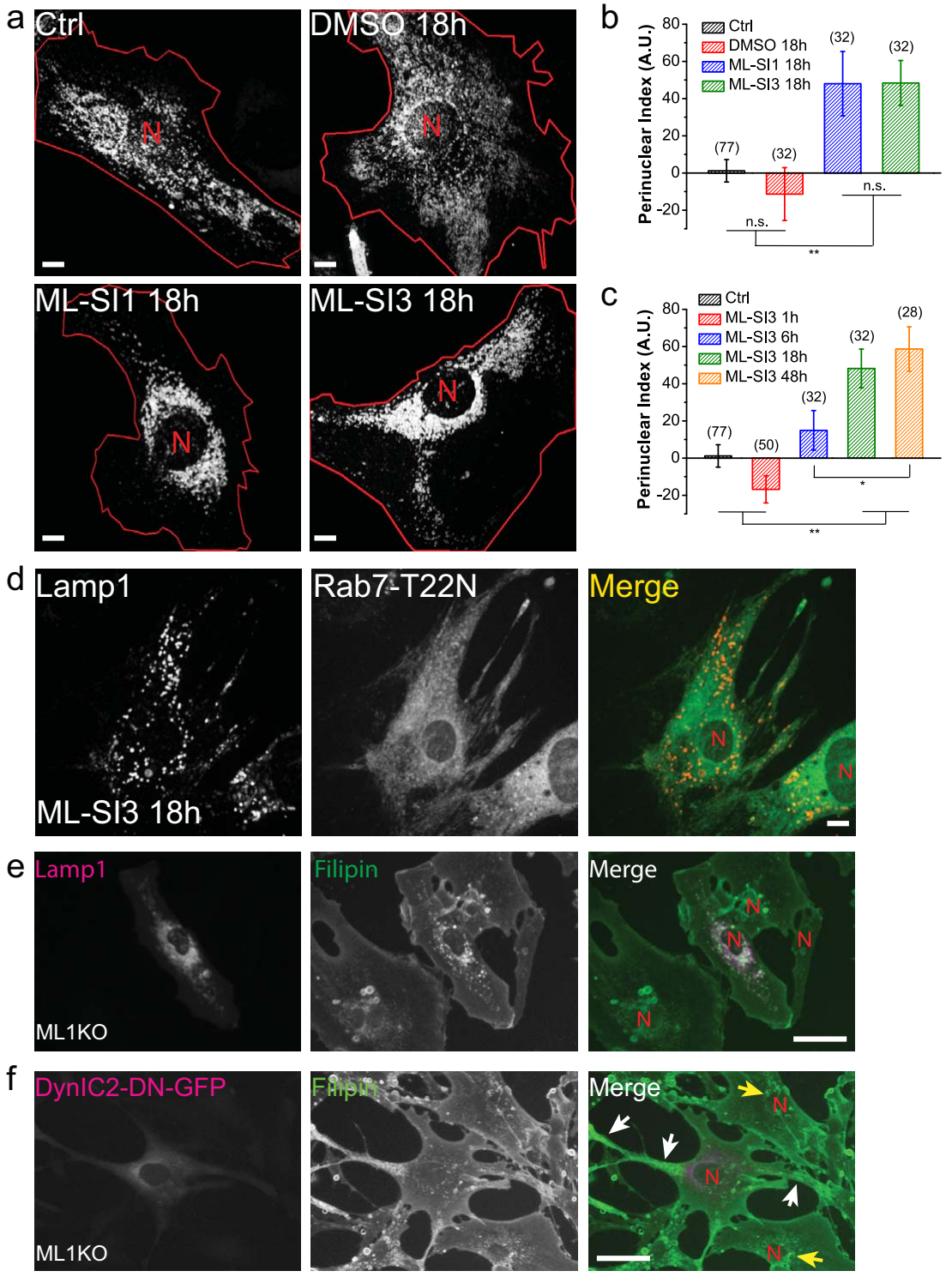

Supplementary Figure 4 Chronic loss of TRPML1 activity causes cholesterol accumulation and perinuclear localization of lysosomes in fibroblasts. (**a**) Lysosome distribution in WT fibroblasts treated with vehicle (0.1% DMSO) (upper right), ML-SI1 25 μM (bottom left), or ML-SI3 25 μM (bottom right) for 18 h in complete medium. (**b**) Quantification of the groups shown in (**a**). (**c**) Time-dependence of TRPML1 inhibition of lysosome distribution in WT fibroblasts in complete medium. (**d**) Representative images showing lysosome distribution in Rab7-T22N-expressing cells in the presence of ML-SI3 (25 μM) for 18 h. (**e**) Representative images showing ML1 KO fibroblasts transfected with Lamp1-mCherry, and stained with filipin. Intracellular puncta filipin staining co-localized well with Lamp1. (**f**) Representative images showing ML1 KO fibroblasts transfected with DynIC2-DN-GFP, and stained with filipin. Graphed data are presented as means ± SEM, the numbers of cells (n) used for quantification were pooled across at least three independent experiments and are shown in the parentheses. $*p < .05$, $**p < .01$ in ANOVA. Scale bars = 10 μm for (**a**) and (**d**), and = 50 μm for (**e**) and (**f**).

© 2016 Macmillan Publishers Limited. All rights reserved

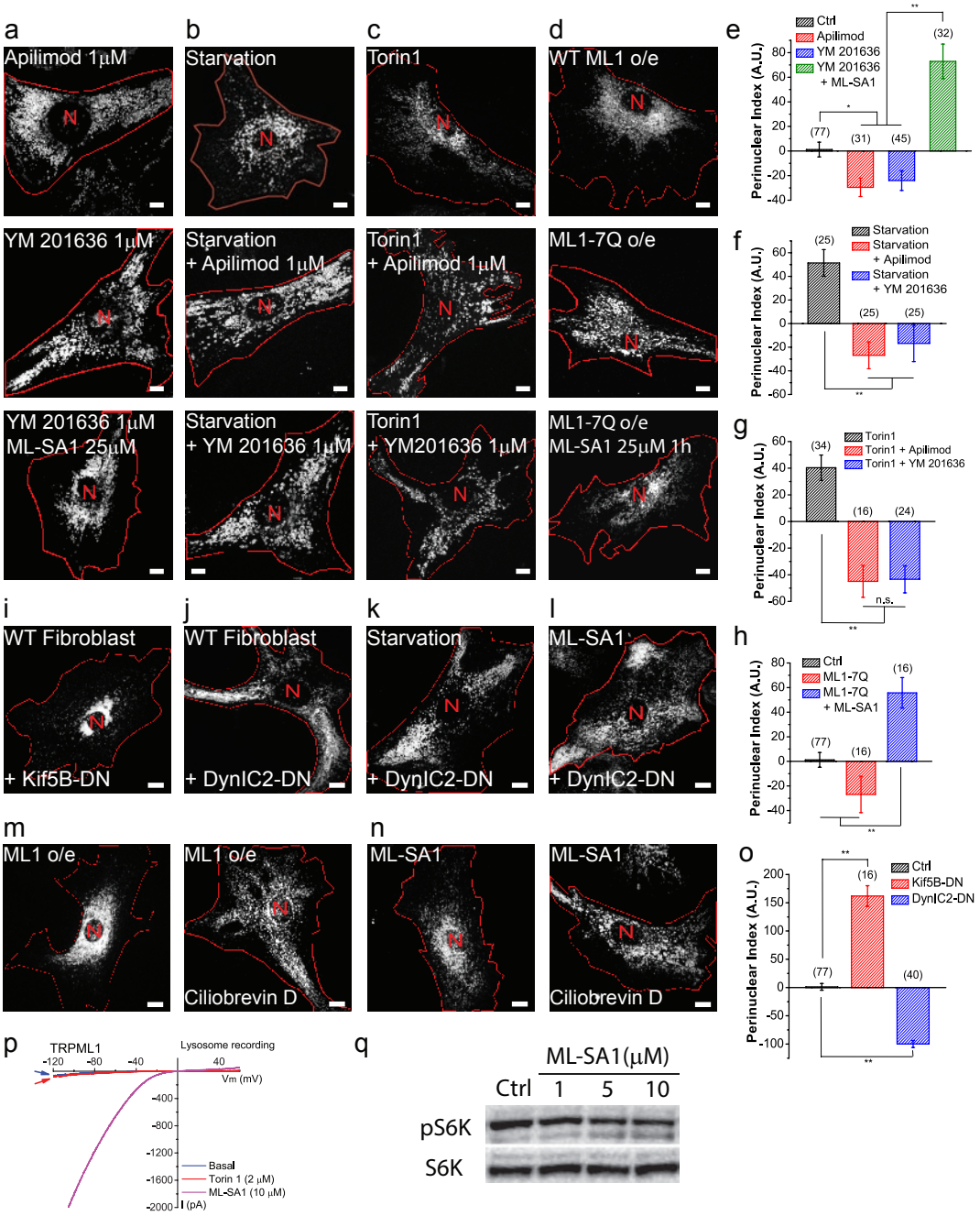

Supplementary Figure 5 Regulation of lysosomes motility by PI(3,5)P_2 and dynein motors. (**a**) Lysosome distribution in WT fibroblasts treated with 1 μM apilimod for 1 h (upper), 1 μM YM 201636 for 1 h (middle), or 1 μM YM 201636 plus 25 μM ML-SA1 for 1 h (bottom). (**b**) Lysosome distribution in WT fibroblasts starved for 1 h (upper), or starved for 1 h in the presence of 1 μM apilimod (middle) or YM 201636 (bottom). (**c**) Lysosome distribution in WT fibroblasts treated with 1 μM Torin-1 for 1 h in the presence of 1 μM apilimod (middle) or YM 201636 (bottom). (**d**) Lysosome distribution in TRPML1-7Q-transfected cells in the presence (bottom) or absence (middle) of 25 μM ML-SA1 for 1 h. (**e**) Quantification of groups shown in (**a**). (**f**) Quantification of groups shown in (**b**). (**g**) Quantification of groups shown in (**c**). (**h**) Quantification of groups shown in (**d**), compared to cells expressing Lamp1 alone. (**i**) Lysosome (labeled with Lamp1-EGFP) distribution in WT fibroblasts transfected with mCherry-tagged dominant-negative Kif5B (Kif5B-DN). (**j-l**) Lysosome (labeled with Lamp1-mCherry) distribution in WT fibroblasts transfected with GFP-tagged dominant-negative cytoplasmic dynein intermediate chain 2 (DynIC2-DN), then left untreated (**j**), starved for 2 h (**k**), or treated with 25 μM ML-SA1 for 2 h (**l**). (**m**) Effect of dynein inhibitor ciliobrevin D (20 μM, 2 h) on lysosome distribution in TRPML1-expressing fibroblasts. (**n**) WT fibroblasts treated with ML-SA1 (25 μM) or together with ciliobrevin D (20 μM) for 2 h. (**o**) Quantification of lysosome distribution in experimental groups shown in (**i**) and (**j**). Red lines outline cell boundaries; "N" marks nuclei. (**p**) Whole-lysosome TRPML1 currents were not activated by Torin-1 in TRPML1-expressing Cos1 cells. ML-SA1 readily activated whole-lysosome TRPML1 currents. (**q**) Application of ML-SA1 (1, 5, 10 μM) in HEK293T cells for 3 h did not lead to a significant change in the level of phophorylated S6K, a major mROTC1 target. Graphed data are presented as means ± SEM, the numbers of cells (n) used for quantification were pooled across at least three independent experiments and are shown in the parentheses). *$p < .05$, **$p < .01$ in ANOVA. Scale bars = 10 μm. Uncropped western blot images are shown in Supplementary Figure 9.

© 2016 Macmillan Publishers Limited. All rights reserved

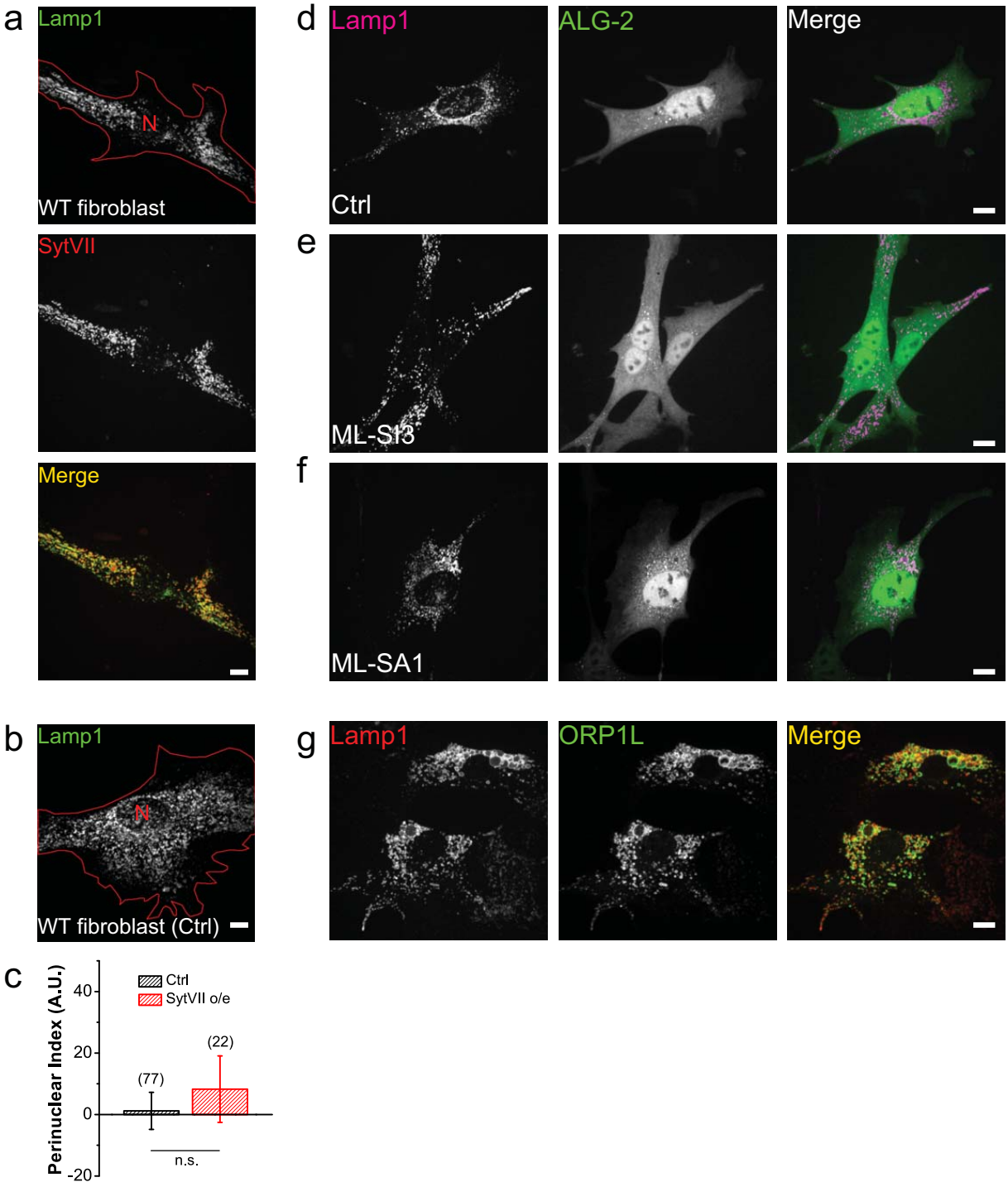

Supplementary Figure 6 Effects of Syt VII, ALG-2, and ORP1L overexpression on lysosome distribution. (**a, b**) WT fibroblasts overexpressing Lamp1-mCherry with (**a**) or without (**b**) Syt VII co-expression. (**c**) Quantification of groups shown in (**a, b**). (**d-f**) WT fibroblasts co-transfected with ALG-2-GFP and Lamp1-mCherry, then left without treatment (**d**), treated with 25 μM ML-SI3 for 2 h (**e**), or treated with 25 μM ML-SA1 for 2 h (**f**). Some perinuclear bright dots of ALG-2 not co-localized with Lamp1 were seen in all treatment conditions. Treatment of ML-SI3 and ML-SA1 resulted in less (ML-SI3) or more (ML-SA1) co-localization with Lamp1 compared to non-treated control cells, respectively. (**g**) ORP1L overexpression induced lysosome clustering as well as enlargement in WT fibroblasts. Red lines outline cell boundaries and nuclei are marked with red "N". Graphed data are presented as means ± SEM, the number of cells (n) used for quantification were pooled across at least three independent experiments and are shown in the parentheses. $*p < .05$, $**p < .01$ in ANOVA. Scale bars = 10 μm.

© 2016 Macmillan Publishers Limited. All rights reserved

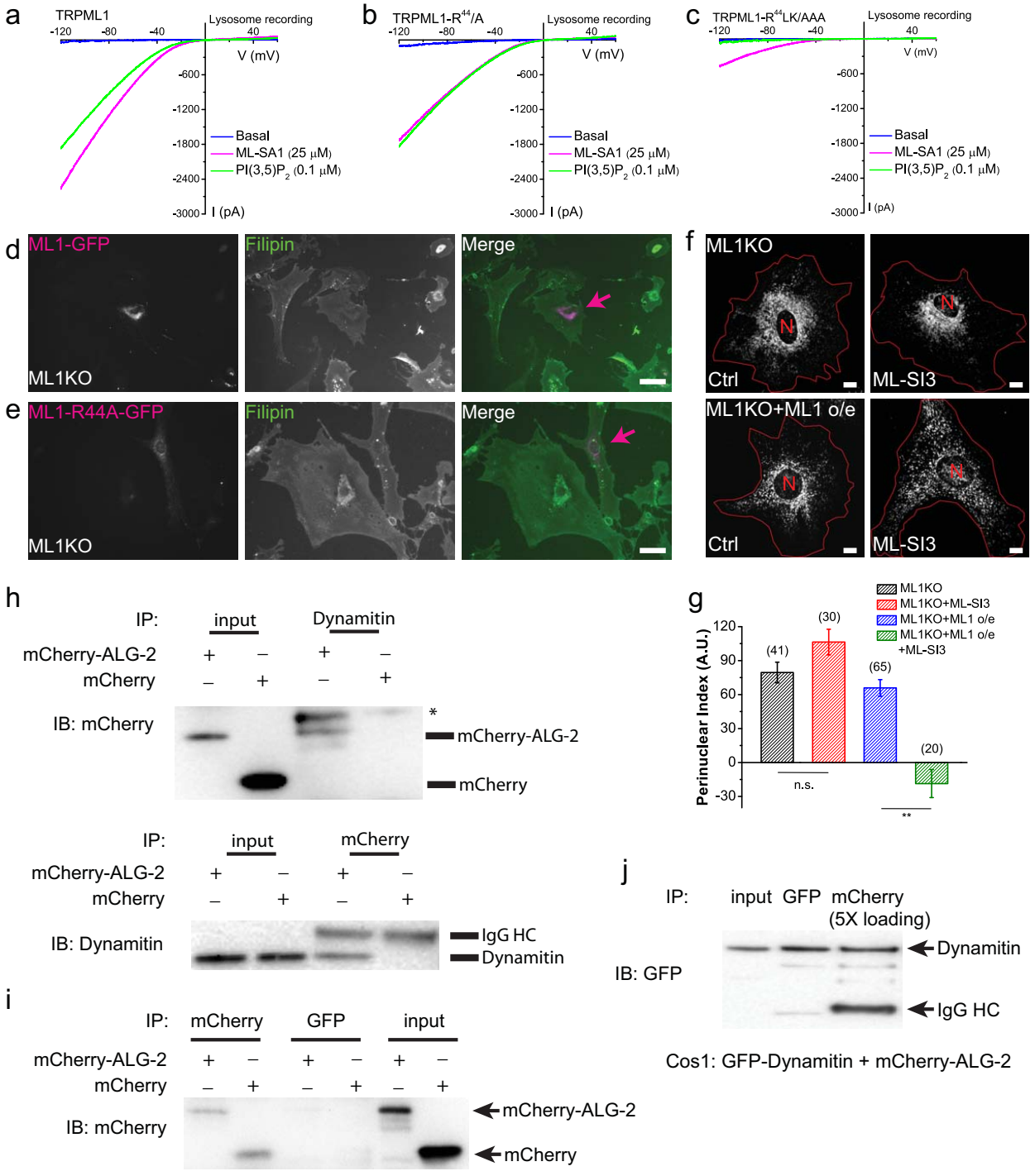

Supplementary Figure 7 ALG-2 mediates the interaction of TRPML1 and dynactin. (**a-c**) Representative whole-lysosome currents in cells overexpressing WT TRPML1 (**a**), TRPML1-R^{44}-A (**b**), or TRPML1-R^{44}LK-AAA (**c**). Whole-lysosome currents were elicited by the endogenous agonist PI(3,5)P_2 or the synthetic agonist ML-SA1. (**d, e**) Filipin staining of *ML1* KO fibroblasts overexpressing TRPML1 (**d**) or TRPML1-R^{44}-A (**e**). Purple arrows indicate cells with overexpression. (**f**) Overexpression of TRPML1 in *ML1* KO fibroblasts causes perinuclear accumulation of lysosomes, but contrary to *ML1* KO fibroblasts without TRPML1 expression, this was reversible through application of 25 μM ML-SI3 for 2 h. (**g**) Quantification of groups shown in (**f**). (**h**) Cells expressing mCherry or mCherry-ALG-2 were subject to Co-IP with either anti-mCherry or anti-Dynamitin, then blotted against mCherry (top) or Dynamitin (bottom). Asterisk indicates a non-specific band seen with HEK293 pull-down. (**i**) Cos1 cells expressing either mCherry or mCherry-ALG-2 were subject to Co-IP with either anti-mCherry or anti-GFP antibodies, then blotted against mCherry. (**j**) Cos1 cells co-expressing GFP-dynamitin and mCherry-ALG-2 were subject to Co-IP with either anti-mCherry or anti-GFP antibodies, then blotted against GFP. Red lines outline cell boundaries and nuclei are marked with a red "N". Graphed data are presented as means ± SEM, the numbers of cells (n) used for quantification were pooled across at least three independent experiments and are shown in the parentheses. *$p < .05$, **$p < .01$ in ANOVA. Scale bars = 10 μm for (**f**), and 50 μm for (**d, e**). Uncropped western blot images are shown in Supplementary Figure 9.

© 2016 Macmillan Publishers Limited. All rights reserved

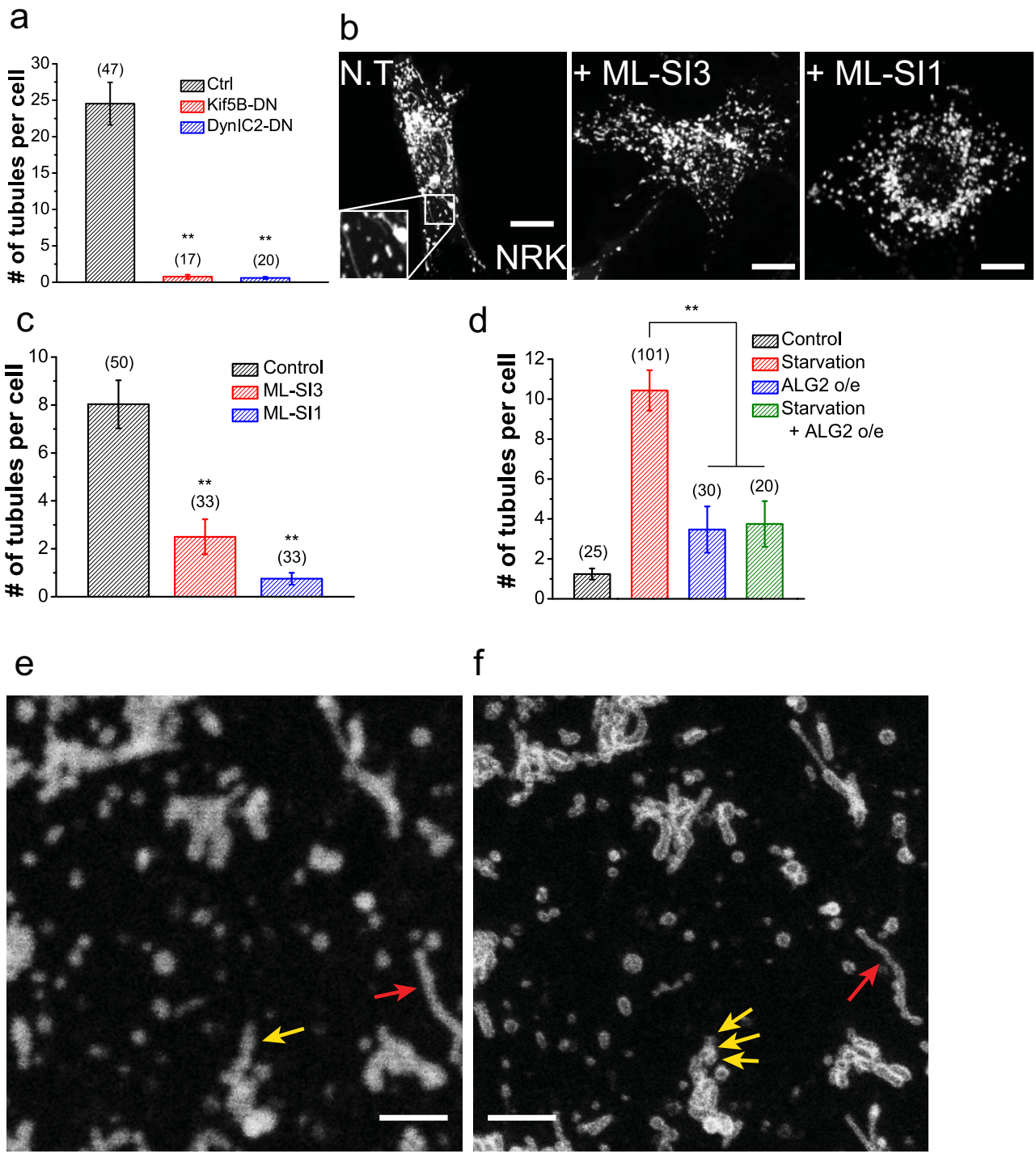

Supplementary Figure 8 Modulation of lysosome tubulation by TRPML1, motor proteins, and ALG-2. (**a**) Quantification of lysosome tubulation in CV-1 cells. Dominant-negative constructs of Kif5B and DynIC2 eliminated spontaneous tubulation in Lamp1-GFP-expressing CV1 cells almost completely. (**b**) Representative images of Lamp1-mCherry-transfected NRK cells starved for 16 h (left), or starved for 16 h with the last 2 h in the presence of 25 μM ML-SI3 (middle) or ML-SI1 (right). (**c**) Quantification of groups shown in (**b**). (**d**) Quantification of lysosome tubulation in WT fibroblasts transfected with Lamp1-GFP, or Lamp1-GFP plus ALG-2-mCherry, with or without starvation for 24 h. ALG-2 expression inhibited lysosome tubulation strongly in starved cells. (**e, f**) Same region of a Lamp1-GFP-transfected fibroblast starved for 24 h under conventional (**e**) or STED super-resolution (**f**) confocal imaging. The super-resolution image was taken 6 s after the conventional confocal image. Yellow arrows point to several small lysosomes that are lined-up to have a tubular appearance under the conventional confocal images; red arrows point to a genuine tubule. Graphed data are presented as means ± SEM, the number of cells (n) used for quantification were pooled across at least three independent experiments and are shown in the parentheses $*p < .05$, $**p < .01$. Scale bars = 10 μm for (**b**), and = 2 μm for (**e, f**).

© 2016 Macmillan Publishers Limited. All rights reserved

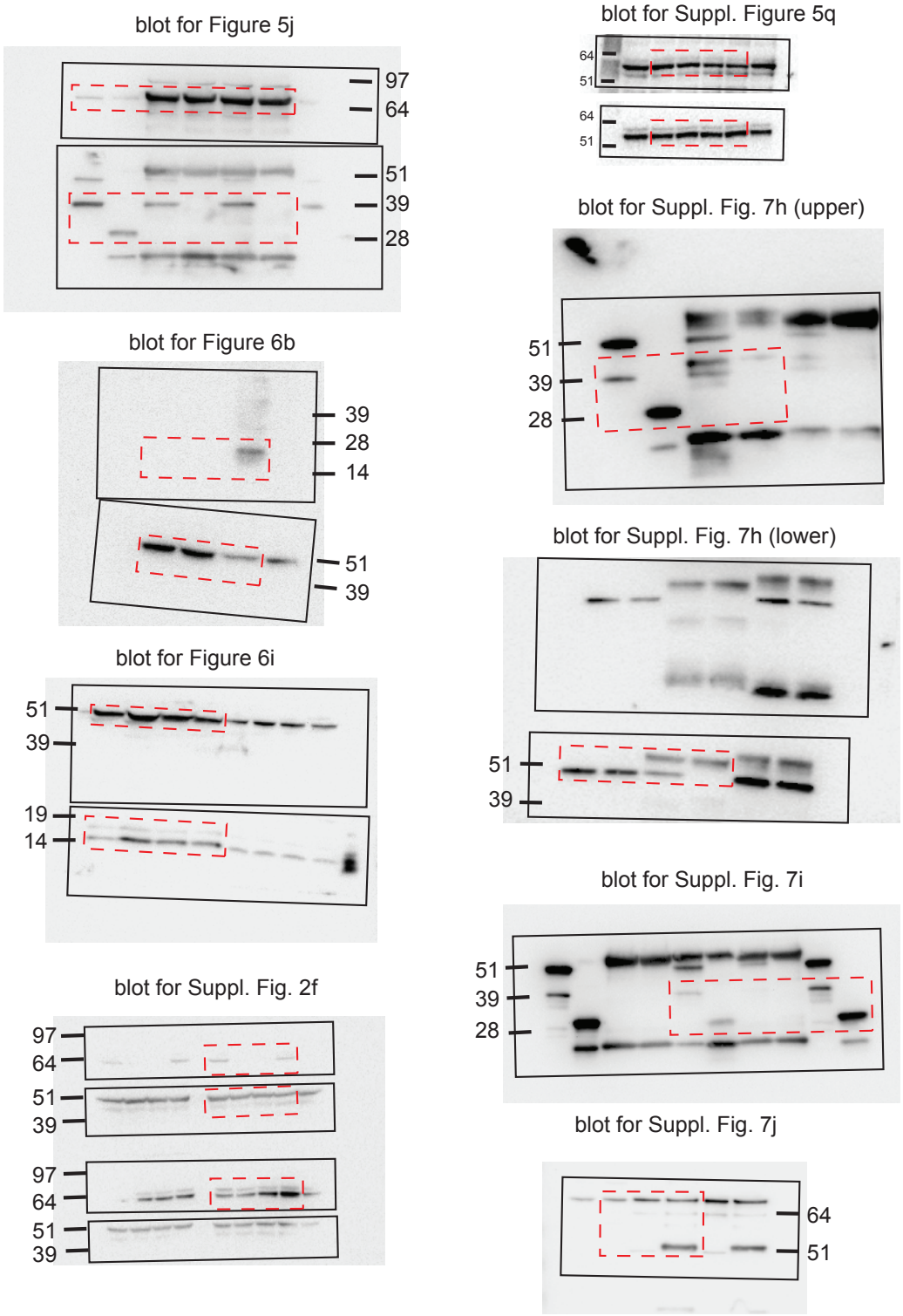

Supplementary Figure 9 Unprocessed scans of original western blots used in the main and supplementary figures. For each image, black boxes indicate roughly the positions of each original blotting membranes, and the red dotted boxes indicate the regions used in the figures. Each image is labeled on top with the panel in the figure they appeared.

© 2016 Macmillan Publishers Limited. All rights reserved

Supplementary video legends

Supplementary Video 1 FRAP analysis of directional movement of lysosomes under normal conditions. Video (1 frame/s) of a Lamp1-mCherry-transfected WT fibroblast. Photobleaching was conducted at the 5th frame (T = 0 s). Scale bar = 10 μm.

Supplementary Video 2 FRAP analysis of directional movement of lysosomes under acute starvation. A Lamp1-mCherry-transfected WT fibroblast imaged 15~30 min after starvation. Scale bar = 10 μm.

Supplementary Video 3 FRAP analysis of directional movement of lysosomes in the presence of the Ca^{2+} chelator BAPTA-AM. Imaging of a Lamp1-mCherry-transfected WT fibroblast after it was incubated with 10 μM BAPTA-AM for 1 h. Scale bar = 10 μm.

Supplementary Video 4 FRAP analysis of directional movement of lysosomes under starvation condition in the presence of ML-SI3. A Lamp1-mCherry-transfected WT fibroblast imaged 15~30 min after starvation in the presence of ML-SI3 (25 μM). Scale bar = 10 μm.

Supplementary Video 5 FRAP analysis of directional movement of lysosomes in the presence of ML-SA1. A Lamp1-mCherry-transfected WT fibroblast imaged 15~30 min after application of ML-SA1 (25 μM). Scale bar = 10 μm.

Supplementary Video 6 Time-lapse imaging of lysosome migration under normal conditions. A Lamp1-mCherry-transfected WT fibroblast was imaged 1 frame/10 s for 250 frames. The video plays 300× real-time speed. Scale bar = 10 μm.

Supplementary Video 7 Time-lapse imaging of lysosome migration upon acute application of ML-SA1. A Lamp1-mCherry-transfected WT fibroblast was imaged at 1 frame/10 s for 250 frames in the presence of 25 μM ML-SA1, which was applied 3 min after the start of the imaging (i.e. frame 18). The video plays 300× real-time speed. Scale bar = 10 μm.

Supplementary Video 8 Time-lapse imaging of lysosome migration in TRPML1-expressing cells upon acute application of ML-SI3. TRPML1-GFP-expressing WT fibroblast was imaged at 1 frame/10 s for 250 frames in the presence of 25 μM ML-SI3, which was applied 3 min after the start of the imaging (i.e. frame 18). The video plays 300× real-time speed. Scale bar = 10 μm.

© 2016 Macmillan Publishers Limited. All rights reserved